The Dissertation Committee for Damon Allen Smith
Certifies that this is the approved version of the following dissertation:

Mechanical, Electromechanical, and Optical Properties of Germanium Nanowires

APPROVED BY
SUPERVISING COMMITTEE:

Supervisor:

Brian A. Korgel

Rodney S. Ruoff

John G. Ekerdt

Paulo J. Ferreira

Emanual Tutuc

Mechanical, Electromechanical, and Optical Properties of Germanium Nanowires

by

Damon Allen Smith, B.S. M.S.

Dissertation

Presented to the Faculty of the Graduate School of

The University of Texas at Austin

in Partial Fulfillment

of the Requirements

for the Degree of

Doctor of Philosophy

The University of Texas at Austin

December 2009

Dedication

To Sarah

Acknowledgements

I would like to thank my advisor, Dr. Brian Korgel, for his mentorship and support during my time here at the University of Texas at Austin. Dr. Korgel gave me the freedom to explore areas interest with a great amount of independence and provided me with valuable guidance along the way.

I would like to acknowledge all of the past and present members of the Korgel group that have taken this journey with me. They provided me with great support and companionship over these last four and a half years. In particular, I would like to thank Vince Holmberg for providing me with the majority of Ge nanowires, XRD, and XPS characterization. In addition, I thank Vince and Mike Rasch for providing me the PEGylated nanowires.

I would like to thank Mike Tiner and Dr. William Lackowski from the Center for Nano- and Molecular Science and Technology (CNM) for their instrument trainings and valuable discussions.

I would also like to thank my undergraduate and master's advisor, Dr. Kevin Stokes, from the Physics department at the University of New Orleans for starting me down the road towards becoming a successful research scientist.

Most importantly, though, I thank my wife, Sarah, for her continued love and support throughout this whole experience.

Abstract

Mechanical, Electromechanical, and Optical Properties of Germanium Nanowires

Damon Allen Smith, PhD

The University of Texas at Austin, 2009

Supervisor: Brian A. Korgel

In order to completely assess the potential of semiconductor nanowires for multifunctional applications such as flexible electronics, nanoelectromechanical systems (NEMS), and composites, a full characterization of their properties must be obtained. While many of their physical properties have been well studied, explorations of mechanical, electromechanical, and optical properties of semiconductor nanowires remain relatively sparse in the literature. Two major hurdles to the elucidation of these properties are: (1) the development of experimental techniques which are capable of mechanical and electromechanical measurements coupled with detailed structural analysis, and (2) the synthesis of high quality nanowires with the high yields necessary to produce the quantities needed for composite fabrication. These issues are addressed in

this dissertation by utilizing the supercritical fluid-liquid-solid (SFLS) synthesis method to produce germanium (Ge) nanowire specimens for mechanical and electromechanical measurements coupled with high-resolution transmission electron microscopy (HRTEM). In addition, excellent dispersibility and large quantities allow for optical measurements of dispersions and composites.

Ge cantilever nanoelectromechanical resonators were fabricated and induced into resonance. From the frequency response, the Young's modulus of the nanowires was determined to be insensitive to diameter and on par with the literature values for bulk Ge. The mechanical quality factors of the resonators were found to decrease with decreasing diameter. The data indicate that energy dissipation from the oscillating cantilevers occurs predominantly via surface losses.

The mechanical strengths of individual Ge nanowires were measured by in situ nanomanipulation in a scanning electron microscope (SEM). The nanowires were found to tolerate diameter-dependent flexural strains more than two orders of magnitude higher than bulk Ge. Corresponding bending strengths were in agreement with the ideal strength of a perfect Ge crystal, indicative of a reduced presence of extended defects. The nanowires also exhibited plastic deformation at room temperature, becoming amorphous at the point of maximum strain.

The optical absorbance spectra of Ge nanowires were measured and found to exhibit spectra markedly different from bulk Ge. Simulations using a discrete dipole approximation (DDA) model suggest that the difference in light absorption results from light trapping within the nanowires.

Table of Contents

List of Tables

List of Figures

Chapter 1: Introduction

1.1 SEMICONDUCTOR NANOWIRES

1.1.1 Background

Semiconductor nanowires are a special class of nanostructures composed of semiconducting materials which have two dimensions at or below 100 nm. Lengths of nanowires can vary from hundreds of nanometers to as long as several millimeters. An enormous amount of research has been put forth to study these materials, due to many novel properties that they possess.[1] For instance, nanowires with diameters below the Bohr-exciton radius exhibit quantum confinement effects which can drastically alter their band structure and, correspondingly, their electronic and optical behavior. In addition, nanowires have exceptionally large surface-to-volume ratios. This means that a large portion of the atoms are located at the surface. Thus, interactions of the nanowire's surface with its environment can cause major changes in its physical properties. This behavior can be exploited for applications in chemical and biological sensing.[1] A major focus of this dissertation is the elucidation of how the size of semiconductor nanowires affects their mechanical, electromechanical, and optical properties.

1.1.2 Synthetic Methods

A variety of methods have been developed to produce nanowires of semiconducting materials. These methods can be placed into one of two fabrication strategies: "Top-down" and "bottom-up". "Top-down" strategies involve subtractive

fabrication methods. As an example, silicon on insulator (SOI) wafers can be used to fabricate silicon (Si) nanowires using electron beam lithography (EBL).[2] In a typical process, polymethyl(methacrylate) (PMMA) is deposited on the SOI wafer by spin-coating and the EBL system is used to define a pattern in the polymer. Wet and plasma etching can then be used to remove material around the EBL-defined patterns leaving Si nanowires on top of a silicon dioxide substrate. While methods such as this are excellent for creating well-defined nanowires and devices with tightly controlled dimensions, they are labor intensive and expensive processes. "Bottom-up" strategies involve the crystallization of one dimensional structures by the directed self-assembly of atoms. Some successful methods for producing nanowires in this manner are the vapor-liquid-solid (VLS), solution-liquid-solid (SLS), and the super critical fluid-liquid-solid (SFLS) growth techniques. VLS growth is probably the most common approach for "bottom-up" growth of semiconductor nanowires.[1,3,4] Vapor phase growth of micron-sized diameter semiconductor whiskers has been in existence since the 1950s. Pearson et al. found that silicon whiskers would grow on the cooler portions of a quartz tube heated with pieces of Si enclosed in the presence of boron tetrachloride and oxygen.[5] In recent years, this concept has been extended to the growth of semiconductor nanowires with diameters attainable below 100 nm. The VLS growth mechanism involves the growth of a nanowire from a small liquid seed droplet located on the surface of a substrate. Atoms from a vapor phase precursor diffuse into the liquid droplet and form an alloy at temperatures above the eutectic point of the seed droplet and precursor materials. Upon saturation, a solid nanowire is grown from the droplet with diameters dictated by the size of the seed.

SLS and SFLS techniques are essentially solution-phase extensions of the VLS growth mechanism. These synthetic methods provide an excellent route for producing scaled up production of large quantities of semiconductor nanowires not achievable with the VLS method. In a typical reaction, nanocrystal seed particles are feed into a solvent at elevated temperatures in the presence of liquid precursors. While this technique is a tremendous breakthrough for producing large quantities of nanowires made from a variety of compound semiconductor materials[6,7], most traditional solvents degrade before reaching the temperatures required for seeded-growth of group IV semiconductors like Si and Ge. The nanowires used in the experiments herein are produced using the SFLS technique developed by Korgel et al. to produce high yields of high quality semiconductor nanowires.[8,9] The method works by maintaining the integrity of the solvent by pressurizing the reaction chamber above the critical point allowing for the necessary eutectic temperature to be reached. The details of this technique are discussed in chapter 2.

1.2 MECHANICAL AND ELECTROMECHANICAL PROPERTIES OF NANOWIRES

1.2.1 Background

The mechanical properties of macroscale crystalline materials are dominated by phenomenon associated with its microstructure. This refers to the material's crystal structure as well as any imperfections such as point, line, and planar defects.[10,11] As we continue to push the limits of device miniaturization, it becomes extremely relevant to

consider if the same mechanisms still hold as a material size is reduced further and further.

The size-dependence of mechanical properties of various materials have actually been studied for many years. One of the most well-known relationships between the size of a material and its mechanical properties is the Hall-Petch relation for polycrystalline solids.[12,13] Hall and Petch discovered that the yield strength of a material depends on the constituent grain sizes. The yield strength increases due to a grain boundary-mediated disruption of dislocation motion. More recently, the relation was discovered to break down at some critical grain size resulting in softening of a material.[14,15]

Early experimental work studying the mechanical properties of single crystal whiskers with micron scale diameters revealed strengths that far exceeded macroscopic specimens which continued to strengthen with decreasing diameters.[16] This size-dependent strengthening effect can be explained by the reduced presence of defects within the whisker due to the limited volume compared to bulk materials. However, even with the increase in strength, they still do not obtain the theoretical strength of a perfect crystal.[17,18] It is, therefore, interesting to consider what happens when single crystals are reduced to the nanoscale.

Nanowires provide excellent test specimens for studying the mechanical properties of single crystals reduced to nanoscale dimensions. Their large aspect ratios allow for attachment to microscale test structures for various mechanical measurements or manipulations. In addition to the potential increases in strength offered by the further reduction in size of the nanowires, the dramatic increase in surface-to-volume ratio may influence the mechanical properties of the nanowire. This increase in surface area can

affect the mechanical properties by creating surface stress due to coordination number deficiency of surface atoms.[19,20] For very small diameters, it is expected that the surface properties will contribute significantly to the mechanical properties of the nanowire.

1.2.2 EXPERIMENTAL TECHNIQUES

A significant amount of experimental and computation work has been undertaken with single and multiwall carbon nanotubes (SWCNTs and MWCNTs)[21] and metal and semiconducting nanowires.[22] However, in many cases the experimental results do not agree with modeling or experimentally measured properties are conflicting for the same material,[22] speaking to the need for further theoretical understanding and improved experimental methods.

The major challenge of determining the mechanical properties of one dimensional nanomaterials is the fabrication or manipulation of the nanostructures onto appropriate test platforms. One of the first methods for testing the mechanical properties of nanowires utilized an atomic force microscope (AFM) to manipulate silicon carbide (SiC) and MWCNTs on silicon dioxide substrates.[23] The nanostructures were pinned at one end by deposition of square pads and the free end was laterally flexed with the AFM probe. A variation of this method using an AFM to perform three-point bend tests on doubly clamped suspended nanostructures has received significant attention.[23-31] Several researchers have also measured mechanical properties through the mechanical- or electric field-induced oscillations of suspended beams along with extraction of physical properties from their frequency-dependent vibration amplitudes utilizing elastic beam

models.[2,32-39] Other methods include tensile testing between two AFM cantilevers and MEMS platforms, and nanoindentation.[40]

An exploration of electric field-induced resonance of Ge nanowire cantilevers and nanomanipulation of individual Ge nanowires inside of a scanning electron microscope (SEM) is utilized in Chapters 3 and 4 to explore their mechanical and electromechanical properties. The experiments are complemented by high resolution transmission electron microscopy (HRTEM) for precise determination of the individual nanowire's dimensions and crystal structure.

1.3 Optical Properties of Semiconductor Nanowires

Electromagnetic interactions with nanostructures having dimensions much less than the wavelength of light are of particular interest for the development of a variety of new photonic applications.[42,43] Semiconductor nanowires have been examined for nanoscale photonic applications because of their ability to concentrate light into subwavelength volumes.[44,45] Nanowires with high refractive index relative to their surroundings can act as nanoscale optical cavities, creating resonant modes capable of propagating light like optical fibers. This effect has been observed in several examples of prototype single nanowire waveguides[46,47], lasers[47,48], and photodetectors.[44,49] In addition, ensembles of nanowires have been shown to have extremely low reflectance and enhanced light absorption by trapping light through multiple scattering events. [50-52] Therefore, films of these materials are promising for antireflective coatings and photovoltaic applications. The optical interactions of these devices depend sensitively on nanowire dimensions, orientation, composition, and morphology, providing an additional

avenue for tunable optical properties for semiconductor nanoparticles larger than the Bohr-exciton radius. An understanding of this phenomenon is important when engineering optical and optoelectronic devices with these materials. In Chapters 5 and 6, the optical properties of solution-phase dispersions, Ge nanowire-polymer composites, and Ge nanowire nanofabrics are explored.

1.4 DISSERTATION OVERVIEW

Studies of the mechanical and electromechanical properties of semiconductor nanowires remain quite sparse in the literature compared to other property characterization. However, these systems offer distinct opportunities for understanding mechanical behavior on the nanoscale and for evaluating their potential in flexible devices and NEMS. Additionally, it is interesting to consider whether these materials might be useful in multifunctional composites or nanofabrics.

The SFLS method has been shown to produce high yields of high quality single crystal Ge nanowires. Chapter 2 describes the synthesis and the methods utilized to stabilize their surfaces through in situ surface passivation with organic ligands. The results produce Ge nanowires in the abundance necessary to explore single wire studies as well as composites and fabrics.

In Chapter 3, germanium nanowire cantilevers are fabricated by the use of a nanomanipulator inside of a dual beam scanning electron microscope / focused ion beam (SEM/FIB) system. Their Young's modulus and mechanical quality factors (Q) are measured as a function of diameter. It is shown that in the nanowire size range investigated the Young's modulus does not change with the size of the diameter and is

comparable to bulk Ge. However, the Q of the nanowires are found to decrease as the diameters of the nanowire cantilevers decrease. The potential mechanical energy dissipation pathways are discussed.

Chapter 4 demonstrates the high strength and large flexibility of the Ge nanowires by in situ nanomanipulation. It is shown that Ge nanowires can tolerate an extremely large bending strain of up to 17 % with the smallest diameter wires able to bend into loops with a 67 nm radius of curvature. The maximum tolerated strain for each nanowire is found to depend on the diameters of the nanowires, indicative of a decrease in defects as the size is decreased. A diameter-dependent strength is also observed with a maximum for an individual wire of 18 GPa, in the range of the theoretical value for a perfect crystalline solid. At extremely large strains without fracture, plasticity is also observed in these wires.

A method to produce Ge nanowire-composite films is demonstrated. It is shown that ensembles of Ge nanowires exhibit absorbance spectra that differ dramatically from bulk Ge. Features of the spectra are explained by light trapping ability of individual nanowires through the presence of resonant modes inside the wire.

Chapter 6 demonstrates the use of vacuum filtration to produce free-standing Ge nanowire mats. A potential application as a type of photoconductive ceramic fabric is explored and discussed.

In the final chapter, Chapter 7, the results are summarized and future directions are discussed.

1.5 REFERENCES

(1) Law, M.; Goldberger, J.; Yang, P. *Annu. Rev. Mater. Res.* **2004**, *34*, 83.

(2) Carr, D. W.; Evoy, S.; Sekaric, L.; Craighead, H. G.; Parpia, J. M. *Appl. Phys. Lett.* **1999**, *75*, 920.

(3) Cui, Y.; Lauhun, L. J.; Gudiksen, M. S.; Wang, J.; Lieber, C. M. *Appl. Phys. Lett.* **2001**, *78*, 2214.

(4) Wu, Y.; Yang, P. *J. Am. Chem. Soc.* **2001**, *123*, 3165.

(5) Pearson, G. L.; Read, W. T.; Feldmann, W. L. *Acta. Metall.* **1957**, *5*, 181.

(6) Fanfair, D. D.; Korgel, B. A. *Cryst. Growth Des.* **2005**, *5*, 1971.

(7) Fanfair, D. D.; Korgel, B. A. *Cryst. Growth Des.* **2008**, *8*, 3246.

(8) Hanrath, T.; Korgel, B. A. *J. Am. Chem. Soc.* **2002**, *124*, 1424.

(9) Hanrath, T.; Korgel, B. A. *Adv. Mater.* **2003**, *15*, 437.

(10) Dowling, N. E. *Mechanical Behaviour of Materials*; Prentice Hall: Englewood Cliffs, NJ, 1999.

(11) Roesler, J.; Harders, H.; Baeker, M. *Mechanical Behaviour of Engineering Materials*; Springer: New York, 2007.

(12) Hall, E. O. *Proc. Phys. Soc. B* **1951**, *64*, 747.

(13) Petch, N. J. *J. Iron Steel Inst.* **1953**, *174*, 25.

(14) Chokski, A. H.; Rosen, A.; Karch, J.; Gleiter, H. *Scr. Metall.* **1989**, *23*, 1679.

(15) Nieman, G. W.; Weertman, J. R.; Siegel, R. W. *Scr. Metall.* **1989**, *23*, 2013.

(16) Evans, C. C. *Whiskers*; Mills and Boon: London, 1972.

(17) Petrovic, J. J.; Hoover, R. C. *J. Mater. Sci.* **1987**, *22*, 517.

(18) Petrovic, J. J.; Milewski, J. V.; Rohr, D. L.; Gac, F. D. *J. Mater. Sci.* **1985**, *20*, 1167.

(19) Cammarata, R. C. *Progr. Surf. Sci.* **1994**, *46*, 1.

(20) Gurtin, M. E.; Murdoch, A. *Arch. Ration. Mech. Anal.* **1975**, *57*, 291.

(21) Qian, D.; Wagner, G. J.; Liu, W. K.; Yu, M. F.; Ruoff, R. S. *Appl. Mech. Rev.* **2002**, *55*, 495.

(22) Park, H. S.; Cai, C.; Espinosa, H. D.; Huang, H. *MRS Bull.* **2009**, *34*, 178.

(23) Wong, E. W.; Sheehan, P. E.; Lieber, C. M. *Science* **1997**, *277*, 1971.

(24) Cuenot, S.; Fretigny, C.; Demoustier-Champagne, S.; Nysten, B. *Phys. Rev. B* **2004**, *69*, 165410.

(25) Heidelberg, A.; Ngo, L. T.; Wu, B.; Phillips, M. A.; Sharma, S.; Kamins, T. I.; Sader, J. E.; Boland, J. J. *Nano Lett.* **2006**, *6*, 1101.

(26) Hoffmann, S.; Utke, I.; Moser, B.; Michler, J.; Christiansen, S. H.; Schmidt, V.; Senz, S.; Werner, P.; Gosele, U.; Gallif, C. *Nano Lett.* **2006**, *6*, 622.

(27) Lukic, B.; Seo, J. W.; Bacsa, R. R.; Delpeux, S.; Beguin, F.; Bister, G.; Fonseca, A.; Nagy, J. B.; Kis, A.; Jeney, S.; Kulik, A. J.; Forro, L. *Nano Lett.* **2005**, *5*, 2075.

(28) Ngo, L. T.; Almecija, D.; Sader, J. E.; Daly, B.; Petkov, N.; Holmes, J. D.; Erts, D.; Boland, J. J. *Nano Lett.* **2006**, *6*, 2964.

(29) Nilsson, S. G.; Borrise, X.; Montelius, L. *Appl. Phys. Lett.* **2004**, *85*, 3555.

(30) Salvetat, J. P.; Andrew, G.; Briggs, D.; Bonard, J. M.; Bacsa, R. R.; Kulik, A. J.; Stockli, T.; Burnham, N. A.; Forro, L. *Phys. Rev. Lett.* **1999**, *82*, 944.

(31) Wu, B.; Heidelberg, A.; Boland, J. J. *Nature* **2005**, *4*, 525.

(32) Chen, C. Q.; Shi, Y.; Zhang, Y. S.; Zhu, J.; Yan, Y. J. *Phys. Rev. Lett.* **2006**, *96*, 075505.

(33) Chen, X.; Zhang, S.; Wagner, G. J.; Ding, W.; Ruoff, R. S. *J. Appl. Phys.* **2004**, *95*, 4823.

(34) Dikin, D. A.; Chen, X.; Ding, W.; Wagner, G.; Ruoff, R. S. *J. Appl. Phys.* **2003**, *93*, 226.

(35) Li, X.; Ono, T.; Wang, Y.; Esashi, M. *Appl. Phys. Lett.* **2003**, *83*, 3081.

(36) Liu, K. H.; Wang, W. L.; Xu, Z.; Liao, L.; Bai, X. D.; Wang, E. G. *Appl. Phys. Lett.* **2006**, *89*, 221908.

(37) Nam, C. Y.; Jaroenapibal, P.; Tham, D.; Luzzi, D. E.; Evoy, S.; Fischer, J. E. *Nano Lett.* **2006**, *6*, 153.

(38) Poncharal, P.; Wang, Z. L.; Ugarte, D.; deHeer, W. A. *Science* **1999**, *283*, 1513.

(39) Sazonanova, V.; Yalsh, Y.; Ustunel, H.; Roundy, D.; Arias, T. A.; McEuen, P. L. *Nature* **2004**, *431*, 284.

(40) Tan, E. P. S.; Lim, C. T. *Compos. Sci. Technol.* **2005**, *66*, 1102.

(41) Ke, C.; Espinosa, H. D. In *Handbook of Theoretical and Computational Nanotechnology*; American Scientific Publishers: 2005.

(42) Agarwal, R.; Lieber, C. M. *Appl. Phys. A-Mater.* **2006**, *85*, 209-215.

(43) Pauzauskie, P. J.; Yang, P. *Mater. Today* **2006**, *9*, 36-45.

(44) Cao, L.; White, J. S.; Park, J. S.; Schuller, J. A.; Clemens, B. M.; Brongersma, M. L. *Nat. Mater.* **2009**, *8*, 643.

(45) Chen, G.; Wu, J.; Lu, Q.; Gutierrez, H. R.; Xiong, Q.; Pellen, M. E.; Petko, J. S.; Werner, D. H.; Eklund, P. C. *Nano Lett.* **2008**, *8*, 1341.

(46) Law, M.; Sirbuly, D. J.; Johnson, J. C.; Goldberger, J.; Saykally, R. J.; Yang, P. *Science* **2004**, *305*, 1269.

(47) Greytak, A. B.; Barrelet, C. J.; Li, Y.; Lieber, C. M. *Appl. Phys. Lett.* **2005**, *87*, 151103.

(48) Johnson, J. C.; Choi, H. J.; Knutsen, K. P.; Schaller, R. D.; Yang, P.; Saykally, R. J. *Nat. Mater.* **2002**, *1*, 106.

(49) Wang, J.; Gudiksen, M. S.; Duan, X.; Cui, Y.; Lieber, C. M. *Science* **2001**, *293*, 1455.

(50) Muskens, O. L.; Diedenhofen, S. L.; Kaas, B. C.; Algra, R. E.; Bakkers, E. P. A. M.; Rivas, J. G.; Lagendijk, A. *Nano Lett.* **2009**, *9*, 930.

(51) Muskens, O. L.; Rivas, J. G.; Algra, R. E.; Bakkers, E. P. A. M.; Lagendijk, A. *Nano Lett.* **2008**, *8*, 2638.

(52) Hu, L.; Chen, C. Q. *Nano Lett.* **2007**, *7*, 3249.

Chapter 2: Supercritical Fluid-Liquid-Solid (SFLS) Synthesis of Germanium Nanowires

2.1 INTRODUCTION

Nanowire growth by the vapor-liquid-solid (VLS) mechanism has been very successful for a variety of different materials, including Group IV, III-V, and II-VI semiconductors, and metal oxides.[1-3] These nanowires can be suspended in solvents for incorporation into devices or deposition of films. However, solution-phase synthesis allows for cheaper and faster production of these nanomaterials.[2]

Due to its prominence in the semiconductor electronics industry, silicon (Si) has received an enormous amount of attention as a material of great interest for nanowire-based applications.[2] However, germanium (Ge) is a particularly interesting material due to it high electron and hole mobility with respect to Si.[4] The large index of refraction and low optical dispersion of Ge make it an interesting material for optical and optoelectronic applications.[5] Moreover, the large Bohr-excition radius permits more accessible quantum confinement effects.[6] Therefore, Ge nanowires offer promising potential for nanoscale devices and composites and further research is needed to truly assess their potential.

Supercritical fluid-liquid-solid (SFLS) growth is utilized herein to produce high quality Ge nanowires and a general overview of the method is provided in this chapter.[7-10] The high precursor solubility allows for high throughput unattainable by VLS methods. For example, more than 1 g of Ge nanowires can be produced in a single reaction carried out in a 250 mL vessel. This approach provides enough material to explore new applications of semiconductor nanowires, like composites and non-woven fabrics explored in Chapters 5 and 6.

2.2 EXPERIMENTAL DETAILS

2.2.1 Gold Nanocrystal Seed Synthesis

Gold (Au) nanocrystals were used as seeds for the SFLS synthesis of Ge nanowires. The gold nanocrystals, passivated with dodecanethiol, were prepared according to the Brust method.[11] For a typical synthesis, 190 mg of hydrogen tetrachloroaurate trihydrate (HAuCl4·3H2O, Aldrich) dissolved in 18 mL deionized water (DI-H2O) was combined with 1.35 g of tetraoctylammonium bromide (TOAB, Aldrich) in 12.5 mL of toluene. The mixture turned to dark brown upon stirring. After 30 minutes, the mixture was separated using a separation funnel and then 120 μL of dodecanethiol (C12H25SH, Aldrich) was introduced to the dark-purple organic phase under stirring. 225 mg of NaBH4 in 15 mL DI-H2O was added dropwise to the organic phase and the reaction was allowed to proceed for 12 hours. The aqueous phase was removed and discarded. Excess ethanol was added to the toluene solution as an antisolvent, and the Au nanocrystals were precipitated by centrifugation for 5 minutes at 5000 rpms. The supernatant was discarded and the nanocrystals were redispersed in anhydrous benzene. The nanocrystals stored inside of a nitrogen-filled glove box.

2.2.2 SFLS Synthesis Apparatus

The SFLS synthesis was performed in a 20 mL titanium flow through reactor. The reactor is placed inside of a heating block and the temperature is controlled with a standard temperature controller. A cylinder filled with anhydrous benzene is connected to an HPLC pump. The HPLC pump drives a piston inside the cylinder used to pressurize the solvent. A second injection cylinder containing the reagents is connected in line between the solvent containing cylinder and the reactor by way of a six-way valve.

A micrometering valve (High Pressure Equipment) at the effluent stream allowed the precise control over the pressure inside the reaction cell.

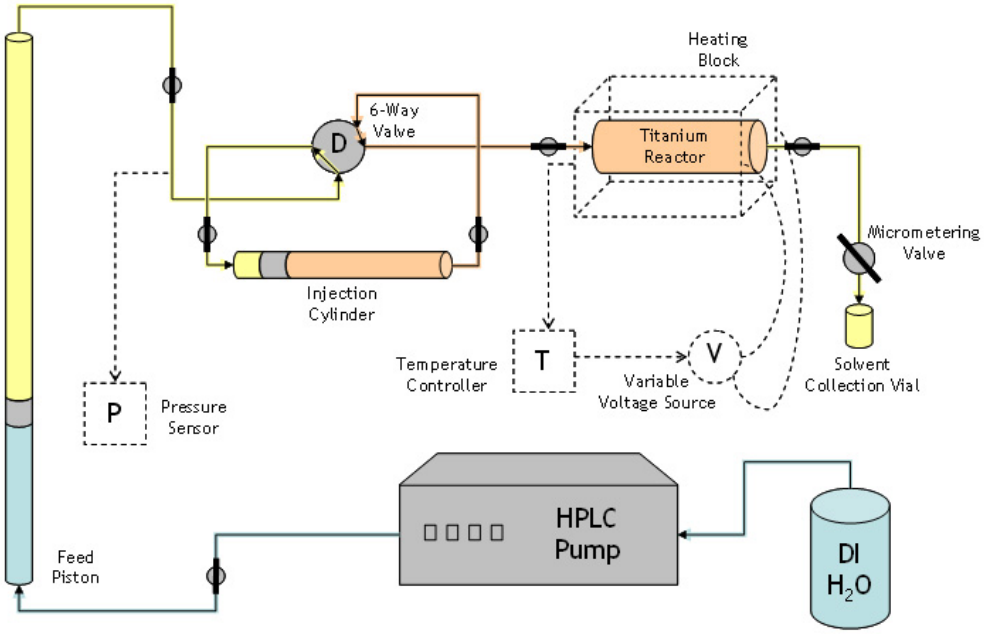

Figure 2.1 Schematic of the experimental setup for the SFLS synthesis. (Courtesy of Vince Holmberg)

2.2.3 SFLS Synthesis of Germanium Nanowires

Ge nanowires were synthesized by the SFLS method using diphenylgermane (Gelest) as a precursor and the gold nanocrystal seeds described in section 2.2.1. A solution of 35 mM diphenylgermane and 16 mg/L dodecanethiol-capped 2 nm diameter Au nanocrystals in anhydrous benzene were injected into a 10 mL titanium reactor at 380°C and 6.3 MPa at a flow rate of 0.5 mL/min. The Ge nanowires were passivated by dodecene, isoprene, or by a PEGylation process. For dodecene or isoprene functionalization, a benzene solution containing 33% dodecene or isoprene by volume

was injected into the reactor and allowed to incubate for 2 hours after stopping injection and cooling the reactor to 220°C. Wires were then dispersed in a toluene solution.

PEGylation of Ge nanowires was accomplished by an intitial functionalization with 11-mercaptoundecanoic acid. A 10 mL solution of 10 volume percent 11-mercaptoundecanoic acid in anhydrous benzene was injected into the reactor at 80^{o}C, causing the thiol groups to react with the Ge surface. After allowing the solution to incubate for 2 hours, followed by cooling to room temperature, the 11-mercaptoundecanoic acid functionalized Ge nanowires were collected and washed in a 2:1:1 volume mixture of chloroform, toluene, and ethanol. This solution was centrifuged at 8000 rpm for 5 min and the precipitated nanowires were redispersed in dimethylsulfoxide. These carboxylic acid terminated Ge nanowires were then further functionalized by activating the terminal carboxylic acid groups with *N*-hydroxysuccinamide (NHS), and adding 1-ethyl-3-(3-dimethylaminopropyl) carbodiimide (EDC) to form a highly reactive intermediate which facilitates the coupling of the activated carboxylic acid group with the amine terminus of a 1000 molecular weight poly(oxyethylene)-poly(oxypropylene) amine polymer, $CH_3(OCH_2CH_2)_{19}(OCH_2CH(CH_3))_3NH_2$, (Jeffamine M-1000). Stock solutions of NHS, EDC, and Jeffamine M-1000 dissolved in dimethylsulfoxide were prepared immediately before reaction. In one example, 4 mg of 11-mercaptoundecanoic acid functionalized Ge nanowires were stirred in 4 mL of dimethylsulfoxide. 25 μmol of NHS and 250 μmol of Jeffamine M-1000 were added to the solution, followed by 25 μmol of EDC. After stirring for 3 hours, the mercaptoundecanoic-amide-polyethyleneglycol functionalized Ge nanowires were precipitated via centrifugation and washed once again using a 2:1:1 volume mixture of chloroform, toluene, and ethanol, and redispersed in dimethylsulfoxide.

2.2.4 Characterization Methods

The Ge nanowires were characterized by high-resolution scanning electron microscopy (HRSEM), high-resolution transmission electron microscopy (HRTEM), and X-ray photoelectron spectroscopy (XPS). HRSEM images were obtained on a field emission LEO 1530 SEM operated at 5 kV. HRTEM was performed using a JEOL 2010F operating at 200kV. For TEM, samples were prepared by dispersing in toluene followed by dropcasting on a lacey carbon grid (Electron Microscopy Sciences, LC200-Cu, Mesh 200). Fast Fourier transforms (FFT) of TEM images were processed by Digital Micrograph (Gatan) software.

2.3 RESULTS AND DISCUSSION

2.3.1 Gold Nanocrystal Synthesis Results

Gold nanocrystals were synthesized with diameter of 2 nm. Figure 2.2 shows a low resolution TEM image of the product of a typical synthesis.

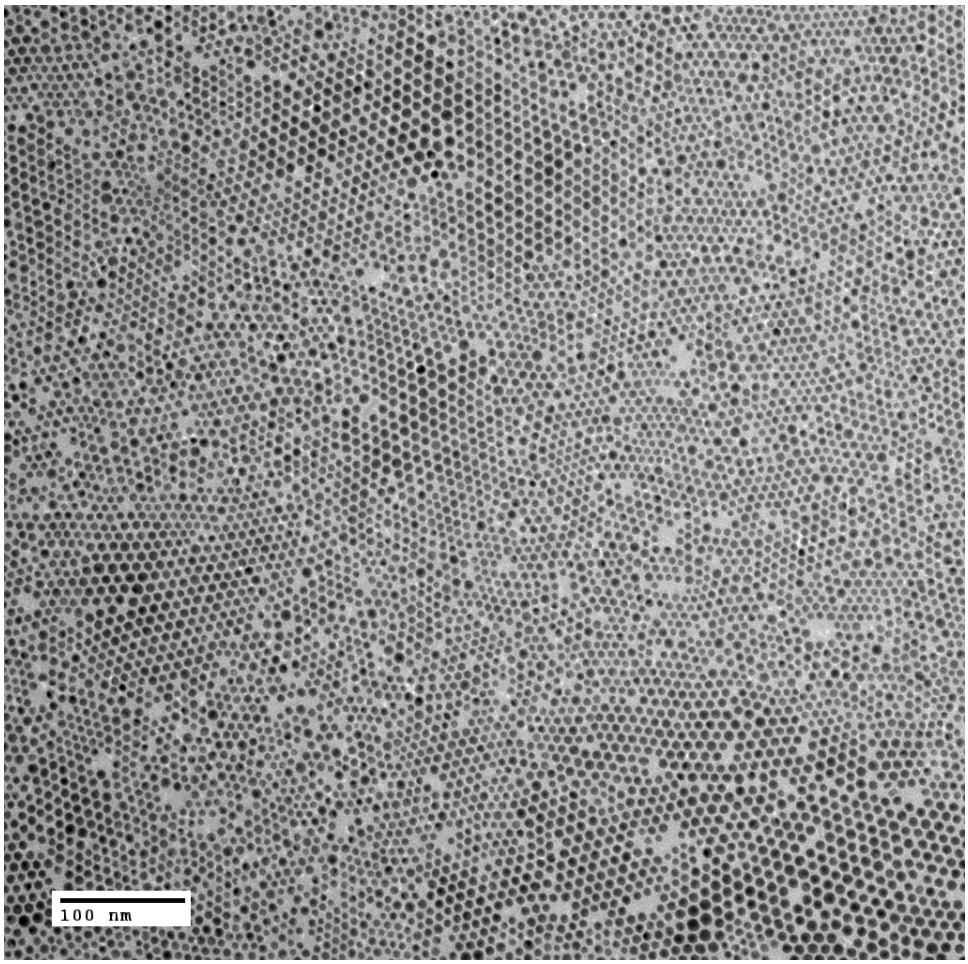

Figure 2.2 TEM image of dodecanthiol-coated gold nanocrystals.

2.3.2 Germanium Nanowire Synthesis Results

The Ge nanowires form by a VLS-like method in super critical benzene.[7,8] Above the eutectic temperature of gold and Ge, Ge atoms from the thermally-degraded Ge precursor diffuse into the gold seed droplet (Figure 2.3). Upon saturation, a solid Ge nanowire is grown from the seed. Figure 2.4 shows representative SEM and HRTEM images of Ge nanowires produced by the SFLS synthesis. Figure 2.5 shows the XRD of wires which have the diamond cubic crystal structure. The growth directions are

primarily in the <111> direction determined from FFTs of HRTEM images. The nanowires formed were up two several microns long (with some reaching mm length scales) with a distribution of diameters between approximately 10-70 nm (Figure 2.6). XPS of surface passivated and unpassivated nanowires (Figure 2.7) taken immediately after synthesis showed Ge3d oxidation peaks reduced for the passivated samples, representative of successful surface coverage and oxidation resistance.

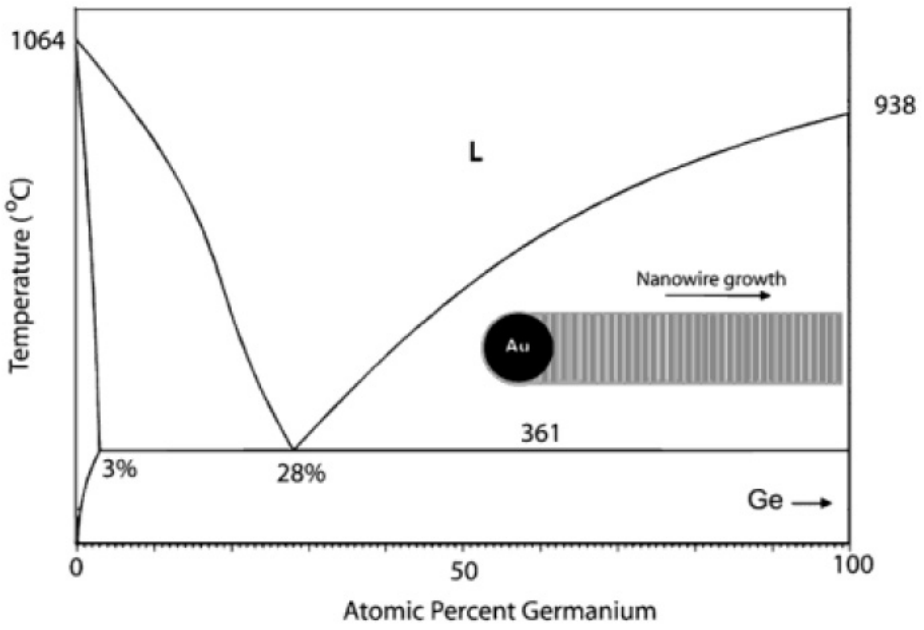

Figure 2.3 Binary phase diagram for Au:Ge. (Courtesy of Ref. 7)

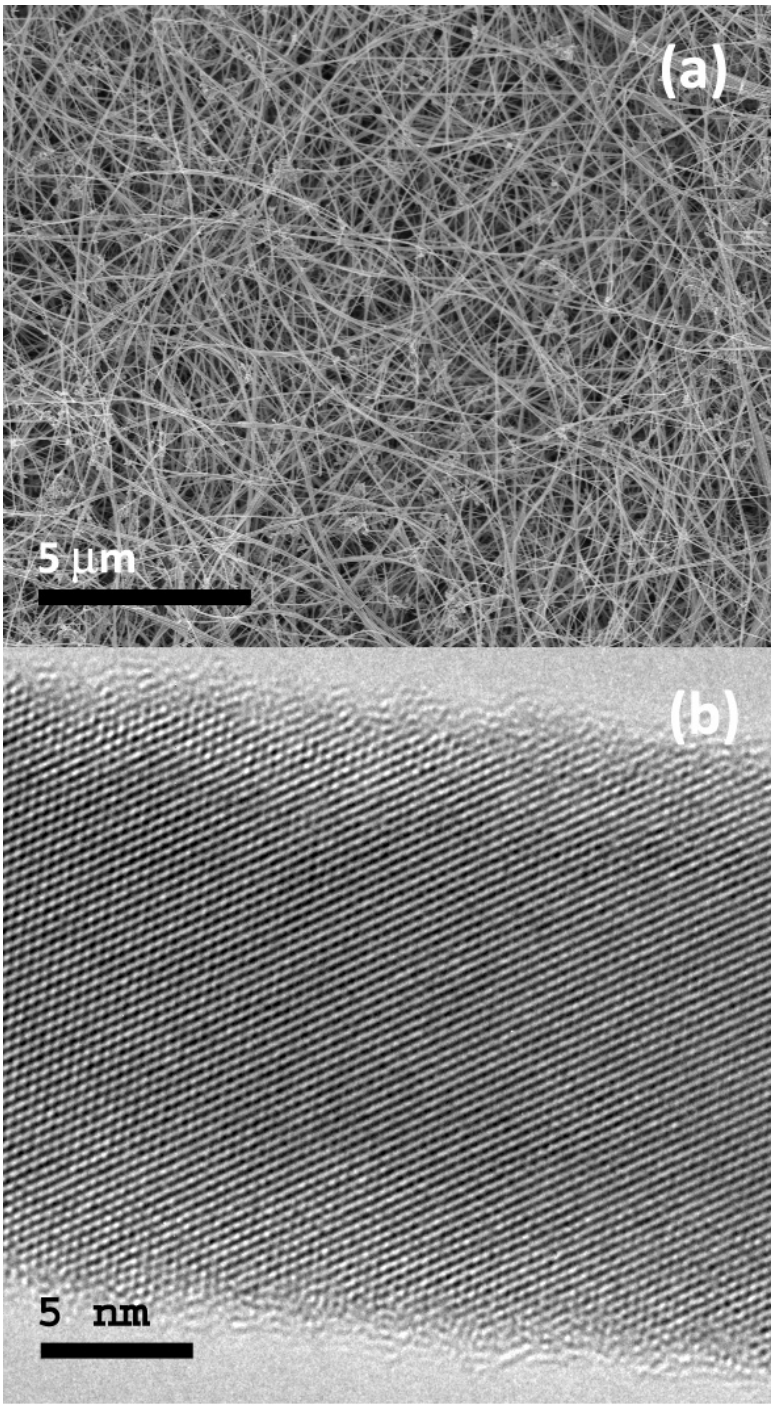

Figure 2.4 (a) SEM and (b) HRTEM image of SFLS-grown Ge nanowires.

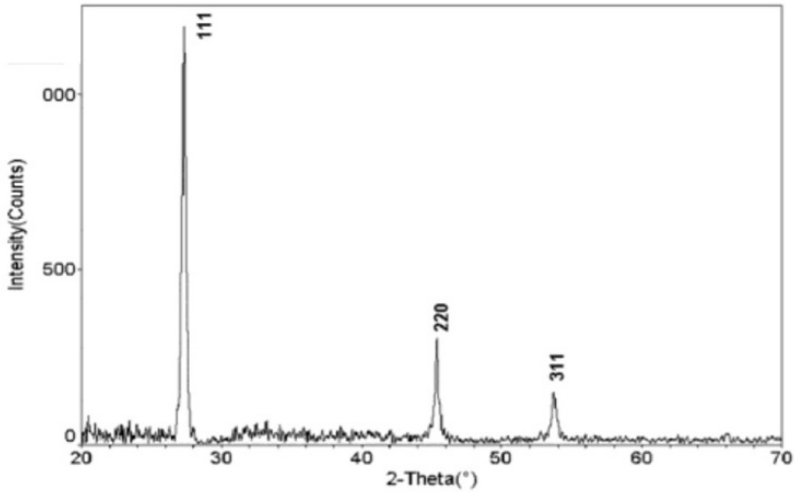

Figure 2.5 XRD pattern of diamond cubic Ge nanowires. (Courtesy of Vince Holmberg)

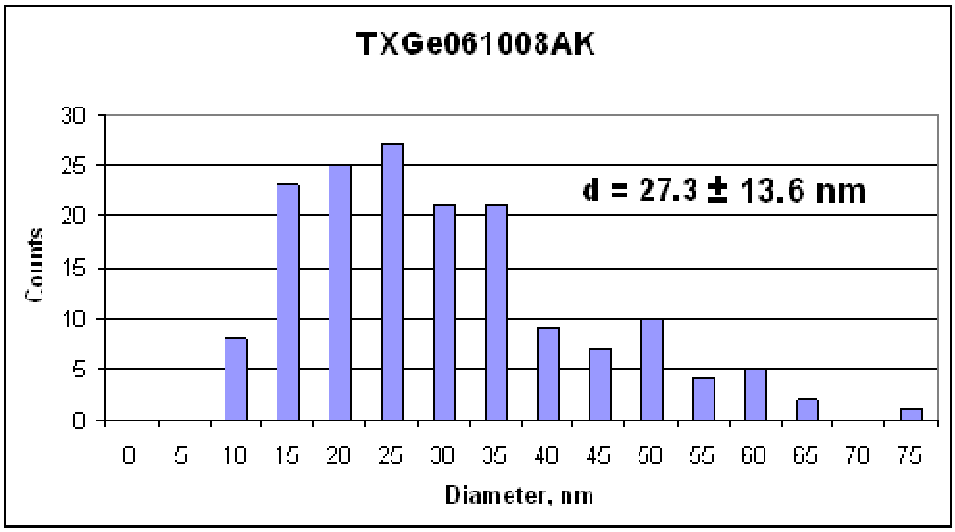

Figure 2.6 Typical Ge nanowire size distribution. (Courtesy of Alex Knoop)

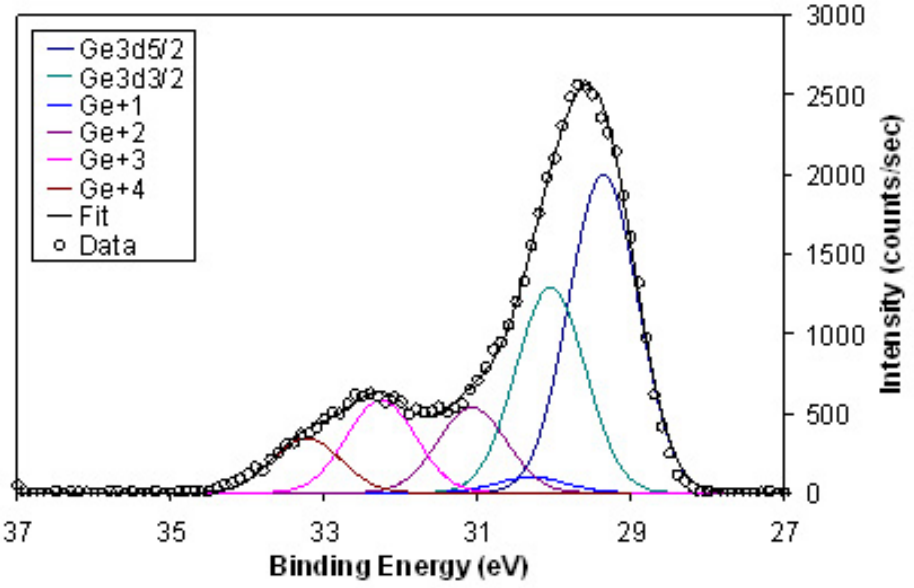

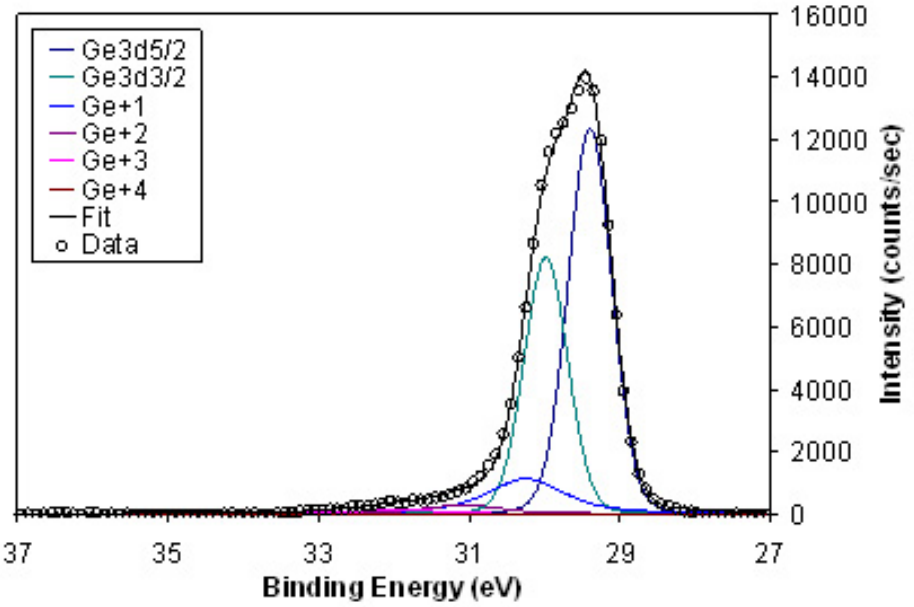

Figure 2.7 Representative XPS data of Ge nanowires (a) without surface passivation and (b) with surface passivation using dodecene. (Courtesy of Vince Holmberg)

2.4 CONCLUSIONS

Thermolytically-degraded diphenylgermane in supercritical benzene produced single crystal Ge nanowires when seeded with dodecanethiol-coated gold nanocrystals. The nanowires obtained were several microns long on average with a diameter distribution between 10 and 70 nm and an average of approximately 30 nm, typically. Very few crystallographic defects were observed with minimal oxidation occurring after surface passivation. The SFLS method of nanowire growth successfully produced large quantities of high quality materials necessary for experimental studies of single nanowires, composites, and fabrics.

2.5 REFERENCES

(1) Cui, Y.; Lauhun, L. J.; Gudiksen, M. S.; Wang, J.; Lieber, C. M. *Appl. Phys. Lett.* **2001**, *78*, 2214.

(2) Law, M.; Goldberger, J.; Yang, P. *Annu. Rev. Mater. Res.* **2004**, *34*, 83.

(3) Wu, Y.; Yang, P. *J. Am. Chem. Soc.* **2001**, *123*, 3165.

(4) Sze, S. M. *Physics of Semicoductor Devices*; John Wiley: New York, 1981.

(5) Claeys, C. *Germanium-Based Technologies: From Materials to Devices*; Elsevier Science: Oxford, 2007.

(6) Maeda, Y.; Tsukamoto, N.; Yazawa, Y.; Kanemitsu, Y.; Masumoto, Y. *Appl. Phys. Lett.* **1991**, *59*, 3168.

(7) Hanrath, T.; Korgel, B. A. *J. Am. Chem. Soc.* **2002**, *124*, 1424.

(8) Hanrath, T.; Korgel, B. A. *Adv. Mater.* **2003**, *15*, 437.

(9) Hanrath, T.; Korgel, B. A. *J. Am. Chem. Soc.* **2004**, *126*, 15466.

(10) Hanrath, T.; Korgel, B. A. *J. Phys. Chem. B* **2005**, *109*, 5518.

(11) Brust, M.; Walker, M.; Bethell, D.; Schiffrin, D. J.; Whyman, R. J. *J. Chem. Soc., Chem. Commun.* **1994**, *801*, 1994.

CHAPTER 3: YOUNG'S MODULUS AND MECHANICAL QUALITY FACTORS OF GERMANIUM NANOWIRE RESONATORS

3.1 INTRODUCTION

Atomic bonding, point defects, and extended defects like dislocations and grain boundaries determine the mechanical properties of crystalline materials. External surfaces do not play a role. In contrast, nanomaterials have a significant fraction of atoms at the surface, which have a different bonding environment than atoms within the bulk solid and therefore the mechanical properties become highly sensitive to surface reconstructions and surface species like adsorbed molecules and coatings.[1-5] The extended defect densities that underlie many mechanical properties of materials (like yield stress and plasticity in particular) are also different since the limited volume of the nanostructure cannot sustain typical defect densities found in bulk materials. This leads to qualitatively different properties, such as toleration of much greater elastic strain.[6] Semiconductor nanowires are expected to have particularly interesting mechanical properties:[7] they are radially confined long cylindrical crystals with nearly infinite periodicity in one dimension and thus have low extended defect densities and very high surface area-to-volume ratios that depend on diameter.[8-14] Their unique mechanical properties also make them interesting candidates for constructing ultrahigh frequency and low power nanoelectromechanical resonators for a variety of different applications.[15]

There have been many reported mechanical property measurements of nanowires, but with widely varying results. For example, the size-dependence of the elastic modulus

of nanowires in similar size ranges with decreasing diameter have been shown to increase (single and multiwall carbon nanotubes[1,16,17] and Ag, Pb, and ZnO nanowires[18,19]), decrease (Cr, Si, and GaN nanowires[20-22]) and remain constant (for multiwall carbon nanotubes and Au and Ge nanowires[23-25]). The wide variability in mechanical property measurements relates in part to the fact that these measurements of individual nanowires present a significant engineering challenge. Nanowires must be fabricated with varying diameter without changes in crystal quality or surface chemistry and then must be effectively integrated into test platforms.

In this chapter, Ge nanowire cantilevers were induced to vibrate by applying a sinusoidal voltage. The natural resonance frequency and the vibration amplitude were measured and then used with elastic beam theory to estimate Young's modulus, *E*. The mechanical quality factor *Q*, was also calculated. *E* was found to be independent of diameter and *Q* decreased with decreasing diameter.

3.2 EXPERIMENTAL DETAILS

3.2.1 Germanium Nanowire Cantilever Fabrication

Ge nanowires were synthesized by gold nanocrystal-seeded supercritical fluid-liquid-solid (SFLS) growth in benzene followed by isoprene surface passivation, using the procedure outlined in Chapter 2. Nanowires were dispersed in chloroform and then deposited onto a lacey carbon TEM grid by drying a drop of the nanowire suspension. The TEM grid was mounted on an SEM stage and placed in an FEI Strata DB235 dual beam scanning electron microscope/focused ion beam (SEM/FIB) system equipped with a Zyvex S100 nanomanipulator. In SEM mode, Ge nanowires were identified that

extended partially over the copper grid and partially over the lacey carbon. The lacey carbon underneath the nanowire was then physically removed using the electrochemically-etched tungsten nanoprobes of the Zyvex S100 nanomanipulator. Platinum was deposited by electron beam-induced deposition (EBID) at the junction between the copper substrate and the Ge nanowire to eliminate slippage of the nanowire during oscillation.

3.2.2 Mechanical Measurements

The nanowire cantilevers were excited into oscillation by applying an AC voltage between two tungsten nanoprobes of the Zyvex S100 nanomanipulator attached to a Solartron 1260A frequency response analyzer (FRA) connected to the probes through a breakout panel outside of the SEM/FIB vacuum chamber. One probe was contacted to the copper grid and the second was held within a micrometer of the nanowire tip. Measurements were carried out by applying a sinusoidal voltage sweep with amplitude of 100 mV. The AC frequency was scanned from 1 kHz and 32 MHz, initially with a 500 Hz resolution until the nanowire was observed to oscillate. The frequency range and resolution were then repeatedly adjusted until the full frequency-dependent amplitude could be observed and approximately 15-25 images of the oscillating nanowire were obtained by SEM. The vibration amplitude was determined using Scion image processing software. The cantilever length was determined from SEM images acquired at several different tilt angles (-15° to 52°). The nanowire diameters were determined by transmission electron microscopy (TEM) on a JEOL 2010F TEM (at a 200kV accelerating voltage).

The Ge nanowire cantilevers were constructed using nanowires ranging from 50 to 140 nm in diameter.[30] Figure 3.1 shows a typical Ge nanowire cantilever. An AC field is applied between an STM tips positioned close to the free end of the nanowire cantilever as shown in Figure 3.1b and an STM tip positioned at the clamped end of the nanowire. As the frequency of the AC field applied between the two STM tips is scanned, the cantilever begins to oscillate as illustrated in Figure 3.1b when it nears the fundamental resonance frequency of the cantilever. The vibrational amplitude of the cantilever as a function of applied frequency was determined from SEM images of the oscillating nanowire.

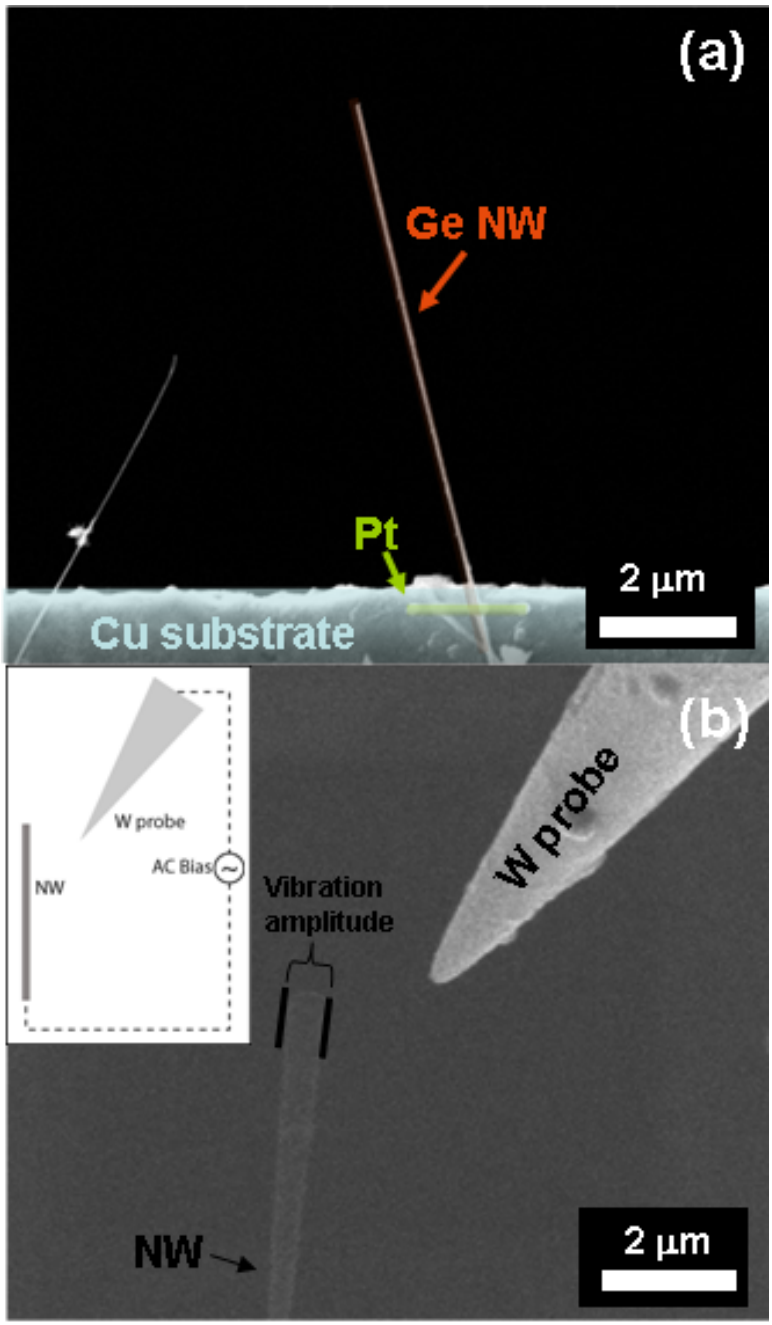

Figure 3.1 (a) SEM image of a Ge nanowire cantilever: the nanowire is glued to the Cu substrate with Pt deposited by electron beam-induced deposition in the SEM/FIB tool. (b) SEM image of an Ge nanowire vibrating in response to a sinusoidal potential applied by the nearby tungsten probe. (Inset) Device schematic.

3.3 RESULTS AND DISCUSSION

Figure 3.2 shows a sample data set for an 88 nm diameter Ge nanowire. The vibrational amplitude varies with frequency and peaks at the natural resonance frequency f_1. f_1 and the full-width-at-half-maximum (FWHM) Δf_1, were determined by fitting the data points with a four-parameter Lorentzian curve. In the range of oscillation amplitudes measured in this study, f_1 is independent of the AC voltage since the amplitudes are more than an order of magnitude less than the cantilever length and therefore satisfies the requirements for application of the Euler-Bernouli equation.[28,31,49]

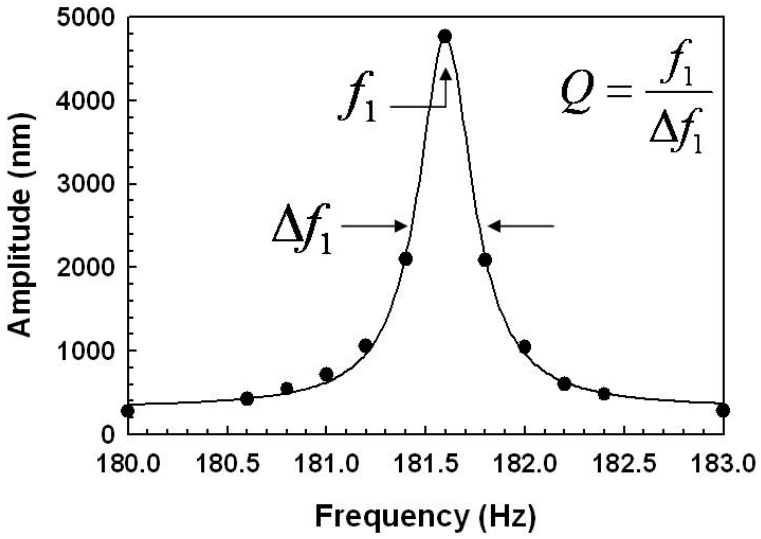

Figure 3.2 Oscillation amplitude determined from SEM images (♦) versus frequency measured for an 88 nm diameter Ge nanowire. The curve is a four-parameter Lorentzian fit to the data: $y = y_0 + a/(1 + ((x - x_0)/b)^2)$ used to determine f_1 and Q. For this nanowire, Q=542 ± 16 and f=181.6 kHz.

Figure 3.3a shows the natural resonance frequency f_1 measured for 14 Ge nanowire cantilevers plotted as a function of the nanowire diameter divided by its length

squared. For a clamped-free beam (i.e., the Euler-Bernoulli model), f_1 depends on the Young's modulus *E*, of the nanowires, and the beam's and length *L*, cross-sectional area moment of inertia I, and mass per unit length m:[31]

$$f_1 = \frac{\beta_1^2}{2\pi}\sqrt{\frac{EI}{mL^4}} \quad . \tag{3.1}$$

The subscript "1" refers to the first resonance mode (i.e., the first eigenmode) of the cantilever, for which $\beta_1 = 1.875$. For a cylindrical beam, $m = \rho(\pi/4)d^2$, where ρ is the density of Ge, and $I = \pi d^4/64$, which yields the expression[31]

$$f_1 = \left(\frac{\beta_1^2}{8\pi}\sqrt{\frac{E}{\rho}}\right) \times \frac{d}{L^2} \quad . \tag{3.2}$$

A plot of f_1 versus d/L^2 in Figure 3.3a gives a straight line, indicating that *E* and ρ do not vary significantly with nanowire diameter in this size range. Fitting Eqn (3.2) to the data in Figure 3.3a gave an average value of *E*=106 GPa with 95% confidence limits of ± 19 GPa. These values correspond to the Young's modulus of Ge down the length of the nanowire, which is predominantly in the <110> direction for these nanowires.[11] This is within the range of the reported values of bulk Ge (*E*=103 to 150 GPa) in the literature.[32-35] Figure 3.3b shows *E* calculated individually for each nanowire using the relation

$$E = 64\rho\left(\frac{\pi f_1}{d}\right)^2\left(\frac{L}{\beta_1}\right)^4 \tag{3.3}$$

E calculated in this way does not vary with nanowire diameter and has an average value of 97 ± 37 GPa, which is slightly less than the value of *E* determined from the plot of f_1 versus d/L^2. Ngo, *et al.*[25] recently reported three-point loading measurements using an

atomic force microscope (AFM) tip to flex individual suspended Ge nanowires (in the same size range) and also observed diameter-independent values of *E* close to the bulk value of Ge.

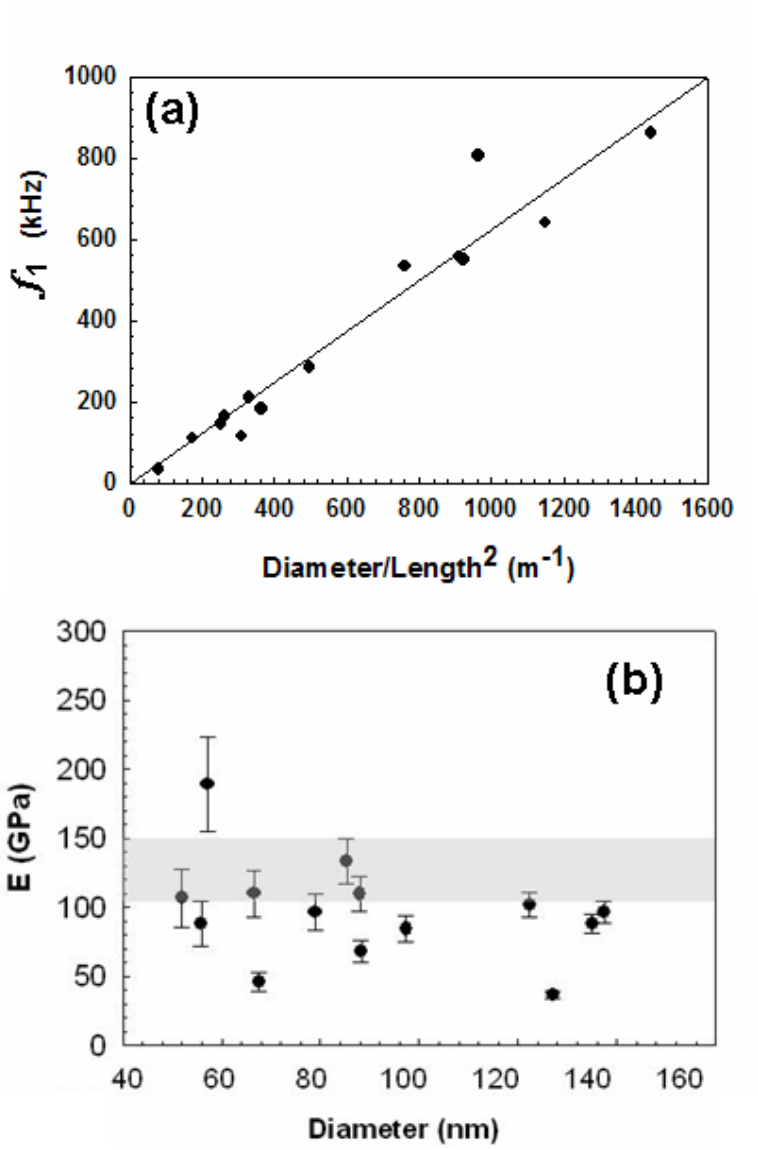

Figure 3.3 (a) Measured values of f_1 plotted versus the nanowire dimensions, d/L^2. A best fit of Eqn (3.2) (—) to the data yields an average value of E=106 GPa with 95% confidence limits of ±19 GPa. (Inset) Diameter-dependence of the measured values of f_1. (b) The Young's modulus E, plotted as a function of nanowire diameter. The shaded region represents the range of values of E for bulk Ge reported in the literature. The value of E was 97 ± 37 GPa.

The mechanical quality factors of the nanowire cantilevers, $Q = f_1/\Delta f_1$,[36] are plotted in Figure 3.4a. Q decreases systematically with decreasing nanowire diameter.

The plot of *Q* versus the cantilever surface area-to-volume ratio (Figure 3.4b) shows the trend of decreasing *Q* with increasing surface area-to-volume ratio, which is well-known for cantilevers fabricated with sub-micrometer diameters, as Carr *et al*.[26] and others[15,37-39] have reported in the literature. The precise reason that *Q* decreases with decreasing diameter of cantilevers in this size range remains a topic of study but it is clear that the energy dissipation related to the surfaces of the crystal is important.

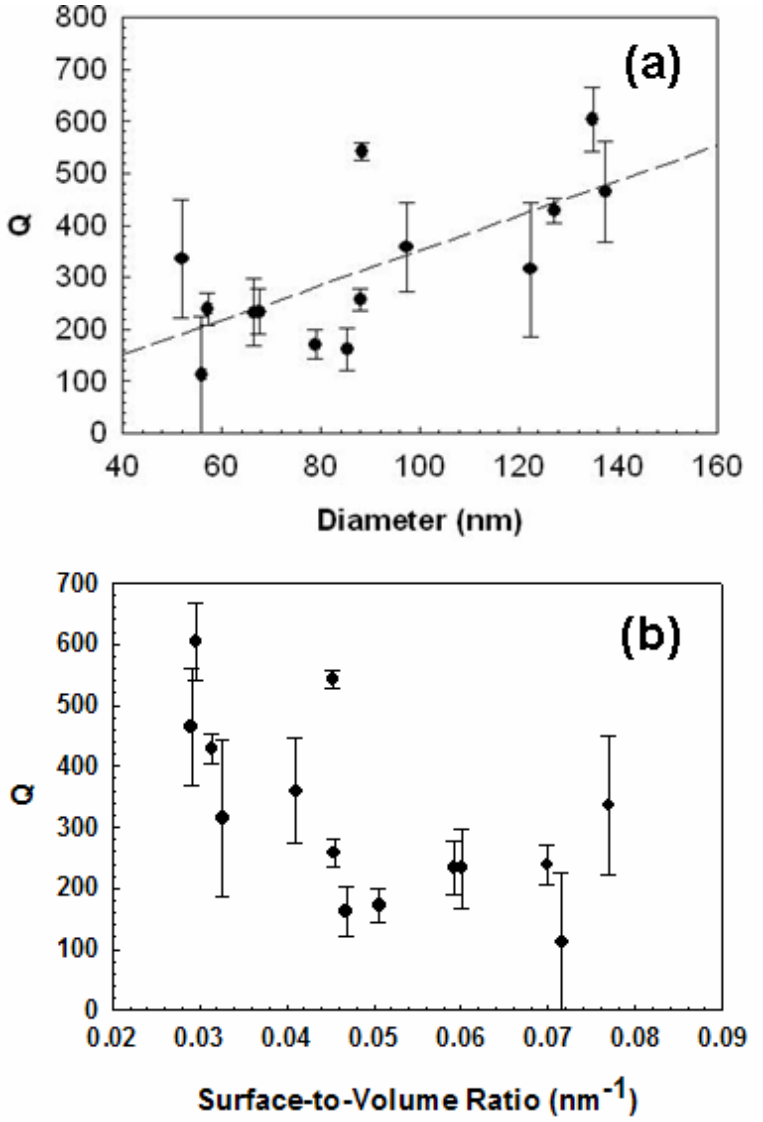

Figure 3.4 (a) *Q* measured for 14 Ge nanowire of different diameter. The dashed line is a a linear extrapolation of the data, provided as a guide to the eye. (b) *Q* plotted versus the surface-to-volume ratio of the nanowires assuming a cylindrical shape.

Q relates inversely to the energy dissipated from the oscillating nanowire.[37] Energy can be lost via multiple pathways *i*, including the support, atmospheric damping,

thermoelastic losses, Ohmic losses, and surface losses, each dissipating a certain amount of energy ΔW_i, per cycle of vibration,[37,38,40,41]

$$Q^{-1} \propto \sum_i \Delta W_i \,. \tag{3.4}$$

In the case of the nanowire cantilevers studied here, the support losses from these high aspect ratio cantilevers are not expected to dominate dissipation.[37,38] Q^{-1} plotted versus cantilever length in Figure 3.5 confirms this expectation, as there is no correlation between Q and the length; however, the shorter cantilevers that are ~10 μm long or less are perhaps exhibiting slightly higher losses from the support than the longer cantilevers.[40] "Atmospheric" damping due to the adsorption of molecules from the surroundings should be negligible because the measurements were conducted in vacuum. Thermoelastic losses (sometimes called "internal friction") should be negligible since the characteristic time for thermal diffusion across the diameter of these thin nanowires greatly exceeds the resonance frequency ($\alpha/d^2 >> 2\pi f_1$, where α is the Ge thermal diffusion coefficient), and the oscillating nanowire retains thermal equilibrium.[41,42] Therefore, the dominant pathway for energy dissipation must relate to the surfaces.

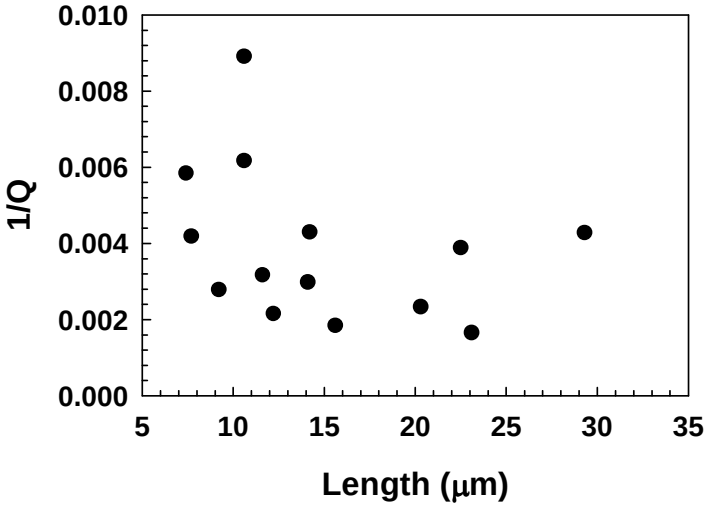

Figure 3.5 1/*Q* versus length of the nanowire cantilevers.

3.3 CONCLUSIONS

The fundamental resonance frequency and mechanical quality factor were measured for Ge nanowire cantilevers with diameters varying from 50 to 140 nm. The Young's modulus was found to be independent of diameter and *Q* decreased with decreasing diameter. The nanowires of differing diameter studied here exhibit no observable difference in crystal quality or surface chemistry. Thus, the mechanical properties related to the Ge-Ge bonding in the core of the wire, such as *E*, do not differ from that of the bulk material when the diameters are in this size range of larger than ~10 nm in diameter, but properties that are very sensitive to the surface, such as the energy dissipation of an oscillating nanowire cantilever (i.e., 1/*Q*), change significantly with the increasing fraction of exposed crystal surface with decreasing nanowire diameter.

High *Q* values are desired for force-sensing applications and therefore surface losses that decrease *Q* with decreasing nanoscale cantilever diameters may be a significant limiting factor in the miniaturization of suspended beam resonators.[15,27,37-39] The Ge nanowires studied here clearly indicate that smaller diameter decreases *Q*, and that this is undoubtedly a fundamental trend of nanometer-scale resonators. The absolute value of *Q*, however, depends strongly on the surface chemistry and surface structure of the cantilever material and wide variations in *Q* have been observed, such as the recent ultrahigh *Q* values of 13,000 measured by Feng, et al.[41] for "pristine" 80 nm diameter Si nanowire cantilevers that are two orders of magnitude higher than the *Q* values of the Ge nanowires studied here. Clearly, the underlying surface chemistry and surface structure underlie how energy dissipates from oscillating nanoelectromechanical resonators and is currently a research topic that requires much greater study and understanding.

3.4 REFERENCES

(1) Lee, K.; Lukic, B.; Magrez, A.; Seo, J. W.; Briggs, G. A. D.; Kulik, A. J.; Forro, L. *Nano Lett.* **2007,** *7*, 1598-1602.

(2) Broughton, J. Q.; Meli, C. A. *Phys. Rev. B* **1997,** *56*, 611-618.

(3) Miller, R. E.; Shenoy, V. B. *Nanotech.* **2000,** *11*, 139-147.

(4) Sharma, P.; Ganti, S.; Bhate, N. *Appl. Phys. Lett.* **2003,** *82*, 535-537.

(5) Lee, B.; Rudd, R. E. *Phys. Rev. B* **2007**, *75*, 195328.

(6) Herring, C. *The Physics of Powder Metallurgy*. McGraw-Hill Book Company, Inc.: New York, 1951.

(7) Herring, C.; Galt, J. K. *Phys. Rev.* **1952,** *85*, 1060-1061.

(8) Davidson III, F. M.; Lee, D. C.; Fanfair, D. D.; Korgel, B. A. *J. Phys. Chem. C* **2007,** *111*, 2929-2935.

(9) Holmes, J. D.; Johnston, K. P.; Doty, R. C.; Korgel, B. A. *Science* **2000,** *287*, 1471-1473.

(10) Korgel, B. A. *Nature Mater.* **2006,** *5*, 521-522.

(11) Hanrath, T.; Korgel, B. A. *J. Am. Chem. Soc.* **2002,** *124*, 1424-1429.

(12) Hanrath, T.; Korgel, B. A. *Adv. Mater.* **2003,** *15*, 437-440.

(13) Shah, P. S.; Hanrath, T.; Johnston, K. P.; Korgel, B. A. *J. Phys. Chem. B* **2004,** *108*, 9574-9587.

(14) Law, M.; Joshua, G.; Yang, P. *Annu. Rev. Mater. Res.* **2004,** *34*, 83-122.

(15) Ekinci, K. L.; Roukes, M. L. *Rev. Sci. Instrum.* **2005,** *76*, 061101.

(16) Poncharal, P.; Wang, Z. L.; Ugarte, D.; de Heer, W. A. *Science* **1999,** *283*, 1513-1516.

(17) Lukic, B.; Seo, J. W.; Bacsa, R. R.; Delpeux, S.; Beguin, F.; Bister, G.; Fonseca, A.; Nagy, J. B.; Kis, A.; Jeney, S.; Kulik, A. J.; Forro, L. *Nano Lett.* **2005,** *5*, 2074-2077.

(18) Cuenot, S.; Fretigny, C.; Demoustier-Champagne, S.; Nysten, B. *Phys. Rev. B* **2004,** *69*, 165410-165414.

(19) Chen, C. Q.; Shi, Y.; Zhang, Y. S.; Zhu, J.; Yan, Y. J. *Phys. Rev. Lett.* **2006,** *96*, 075505.

(20) Li, X.; Ono, T.; Wang, Y.; Esashi, M. *Appl. Phys. Lett.* **2003,** *83*, 3081-3083.

(21) Nam, C.-Y.; Jaroenapibal, P.; Tham, D.; Luzzi, D. E.; Evoy, S.; Fischer, J. E. *Nano Lett.* **2006,** *6*, 153-158.

(22) Nilsson, S. G.; Borrise, X.; Montelius, L. *Appl. Phys. Lett.* **2004,** *85*, 3555-3557.

(23) Wong, E. W.; Sheehan, P. E.; Lieber, C. M. *Science* **1997,** *277*, 1971-1975.

(24) Wu, B.; Heidelberg, A.; Boland, J. J. *Nature* **2005,** *4*, 525-529.

(25) Ngo, L. T.; Almecija, D.; Sader, J. E.; Daly, B.; Petkov, N.; Holmes, J. D.; Erts, D.; Boland, J. J. *Nano Lett.* **2006,** *6*, 2964-2968.

(26) Sazonanova, V.; Yalsh, Y.; Ustunel, H.; Roundy, D.; Arias, T. A.; McEuen, P. L. *Nature* **2004,** *431*, 284-287.

(27) Carr, D. W.; Evoy, S.; Sekaric, L.; Craighead, H. G.; Parpia, J. M. *Appl. Phys. Lett.* **1999,** *75*, 920-922.

(28) Liu, K. H.; Wang, W. L.; Xu, Z.; Liao, L.; Bai, X. D.; Wang, E. G. *Appl. Phys. Lett.* **2006,** *89*, 221908.

(29) Tan, E. P. S.; Lim, C. T. *Compos. Sci. Technol.* **2005,** *66*, 1102-1111.

(30) Nanowires smaller than 50 nm in diameter are obtained in the synthesis, however, these nanowires were unable to withstand the force of pulling away the underlying carbon film and would break during this process and therefore were not studied.

(31) Meirovitch, L. *Analytical Methods in Vibrations*. The Macmillan Company: New York, 1967.

(32) Borchi, E.; Gennaro, S. D.; Macii, R.; Zoli, M. *J. Phys. D: Appl. Phys.* **1988,** *21*, 1304-1305.

(33) McSkimin, H. J. *J. Appl. Phys.* **1953,** *24*, 988-997.

(34) Wortman, J. J.; Evans, R. A. *J. Appl. Phys.* **1965,** *36*, 153-156.

(35) Some of the variation observed in *E* between samples might relate to a difference in nanowire growth direction. High resolution TEM could not be used to directly determine the growth direction of the nanowires after the cantilever was fabricated because the nanowire is not sufficiently stable under the electron beam for high resolution imaging. Statistical analysis of the nanowire growth directions in the sample showed that the majority of the wires used in the study had <110> growth directions, however, some of the nanowires in the sample exhibit <111> and <211> growth directions and it is possible that some of the cantilevers were constructed with nanowires with these other growth directions. Calculations of the Young's modulus have shown a difference of 17 GPa for the <110> and <111> crystal directions in bulk Ge.[33]

(36) Fowles, G. R.; Cassiday, G. R. *Analytical Mechanics*. Hartcourt, Inc.: Florida, 1999.

(37) Yasumura, K. Y.; Stowe, T. D.; Chow, E. M.; Pfafman, T.; Kenny, T. W.; Stipe, B. C.; Rugar, D. *J. Microelectromech. S.* **2000,** *9*, 117-125.

(38) Yang, J.; Ono, T.; Esashi, M. *J. Microelectromech. S.* **2002,** *11*, 775-783.

(39) Gaspar, J.; Chu, V.; Conde, J. P. *Appl. Phys. Lett.* **2004,** *84*, 622-624.

(40) Feng, X. L.; Rongrui, H.; Yang, P.; Roukes, M. L. *Nano Lett.* **2007,** *7*, 1953-1959.

(41) Cimalla, V.; Niebelschutz, F.; Tonisch, K.; Foerster, C.; Brueckner, K.; Cimalla, I.; Friedrich, T.; Pezoldt, J.; Stephan, R.; Hein, M.; Ambacher, O. *Sens. Actuators, B* **2007,** *126*, 24-34.

(42) Zener, C. *Phys. Rev* **1938,** *53*, 90-99.

(43) Ibach, H. *J. Vac. Sci. Technol. A* **1994,** *12*, 2240-2245.

(44) Yang, J.; Ono, T.; Esashi, M. *Appl. Phys. Lett.* **2000,** *77*, 3860-3862.

(45) Wang, Y.; Henry, J. A.; Debodhonyaa, S.; Hines, M. A. *Appl. Phys. Lett.* **2004,** *85*, 5736-5738.

(46) Hanrath, T.; Korgel, B. A. *J. Phys. Chem. B* **2005,** *109*, 5518-5524.

(47) Hanrath, T.; Korgel, B. A. *Small* **2005,** *1*, 717-721.

(48) Feng, et al.[40] state that their Si nanowires had <111> growth directions and faceted {112} surfaces. The Ge nanowires studied here have predominantly <110> growth directions, which have predominantly {111} and {100} faceted surfaces.[47]

(49) An additional requirement for using the Euler-Bernoulli model to calculate the Young's modulus, is to distinguish the fundamental resonance frequency from other higher-order vibrational modes. Forced resonance occurs at $\omega = \omega_0$ and $\omega = \omega_0 / 2$, while parametric resonance occurs at $\omega = \omega_0$ and $\omega = 2\omega_0$, where ω is the angular frequency of the applied voltage ($\omega = 2\pi f$), ω_0 is the natural angular resonance frequency of the nanowire, and n is an integer greater than one.[29] By applying the potential with the counter-electrode transverse to the nanowire, where forced excitation is dominant[18,26] the natural resonance frequency was easily determined.

Chapter 4: Germanium Nanowire Flexibility and Strength Determined by In Situ Nanomanipulation

4.1 INTRODUCTION

Germanium (Ge), like nearly all known ceramics, is a brittle material.[1] Only at high temperature—greater than 350^{o}C—does it exhibit any measurable ductility.[2] This is because plastic deformation requires the nucleation and movement of dislocations, which is largely blocked by the directional, covalent bonding between germanium (Ge) atoms (the Peierls force). Therefore, unless the temperature is very high, a bulk crystal of Ge fractures when deformed just past its yield point.[3] Furthermore, Ge tends to be relatively fragile, with fracture strengths at room temperature (40-95 MPa) that are orders of magnitude less than the ideal strength of 14-20 GPa expected for a perfect Ge crystal.[4,5] A real (bulk) crystal has a variety of nearly unavoidable defects and stresses that serve as sources for crack formation and propagation. Nanowires do not have these same defects and stresses because of their limited size and high surface area to volume ratios, and have been observed to exhibit fracture strengths near those of an ideal perfect crystal.[6-9,2,10,11] Nanowires are also not large enough to sustain dislocations in the same way that bulk crystals do, further leading to rather dramatic differences in mechanical properties. For example, plastic deformation has been observed in Si nanowires at room temperature.[12,13]

Table 1 shows a list of selected materials and their room temperature mechanical properties of elastic modulus, tensile strength, failure strain, and strength-to-weight ratio. There has been a tremendous amount of attention on single- and multiwall carbon

nanotubes as new structural reinforcements because of their incredibly high strength-to-weight ratio. But carbon nanotubes—particularly single wall tubes—remain relatively expensive and can be very difficult to disperse in polymers or other composite host materials.[15] Semiconductor nanowires, like Ge, should also exhibit very high strength-to-weight ratios—on par with Kevlar. Furthermore, nanowires can be dispersed relatively easily in various organic solvents by coating their surfaces with organic ligands.[9] Nonetheless, there has been much less attention paid to these materials for structural applications, primarily because in the past there was a lack of synthetic methods to make them in large quantities.

Table 4.1 Mechanical properties (measured) of selected fibers, nanotubes, and nanowires.

material	elastic modulus (GPa)	tensile strength (GPa)	failure strain (%)	strength-to-weight ratio (kN·m/kg)
Kevlar 49[a]	125	3.5	2.3	24.3
Nomex[a]	10	0.5	22	3.6
E-glass[a]	75	3.5	4	13.6
Aluminum Oxide[a]	350-380	1.7	-	4.6
Carbon Fiber T-300[a]	235	3.2	1.4	18.2
Carbon Fiber M60J[a]	585	3.8	0.7	19.6
Stainless Steel (18-8)[a]	198	1.0-1.4	-	1.8
Tungsten[a]	360	5.5	-	0.28
SWCNT/MWCNT[b]	~1000	11-63	5-12	85-485
Si nanowire[c]	187	12	7	51.5
Ge nanowire	106[d]	18[e]	17[e]	33.8[e]

[a] From reference 11.
[b] From reference 15.
[c] From reference 16.
[d] From reference 17.
[e] This Study.

There are many mechanical property measurements of individual nanowires in the literature,[20,23] but there is still a need for accurate quantitative measurements, and many questions remain with respect to their mechanical properties. In this chapter, individual SFLS-grown Ge nanowires are tested under large flexural strain to determine their maximum strain and fracture strengths by use of a nanomanipulator in an SEM for simultaneous imaging and mechanical testing under high flexural strain.[24] Other commonly used mechanical tests, which include bend tests in an atomic force microscope

(AFM)[10,20,25,26] and fabrication of nanowire cantilevers for electric field-induced resonance testing,[16,27] only work well for examining the elastic properties of the nanowires, and are difficult to use for determining properties like the limit of flexibility and bending strength. It is shown that Ge nanowires exhibit room temperature plasticity under certain bending conditions, enabled by an unusual mechanism of lattice amorphization.[14] (These Ge nanowires also exhibit ideal strengths).

4.2 EXPERIMENTAL DETAILS

4.2.1 Sample Preparation

The nanowires range from 23 to 97 nm in diameter and are crystalline with diamond cubic Ge structure. Mechanical tests were performed on nanowires drop-cast from a chloroform dispersion onto TEM grids coated with a SiN membrane arrayed with 2 μm diameter holes (DuraSiN^{TM}). In the SEM, a nanowire spanning a hole in the membrane was located and then tested.

4.2.2 Mechanical Measurements

The nanomanipulator was used to break a suspended nanowire on one end close to the membrane with an electrochemically-sharpened tungsten probe. The nanowire was bent parallel to the focal plane using two tungsten probes to get an accurate determination of the bending radius. Video of specimen manipulation was obtained by splitting the monitor signal and capturing on a separate computer using a VGA2USB VGA capture device from epiphan systems inc. The video was recorded at a frame rate faster than the

SEM scan rate of 0.34 seconds. Figure 4.1 shows an example of a typical manipulation of a nanowire.

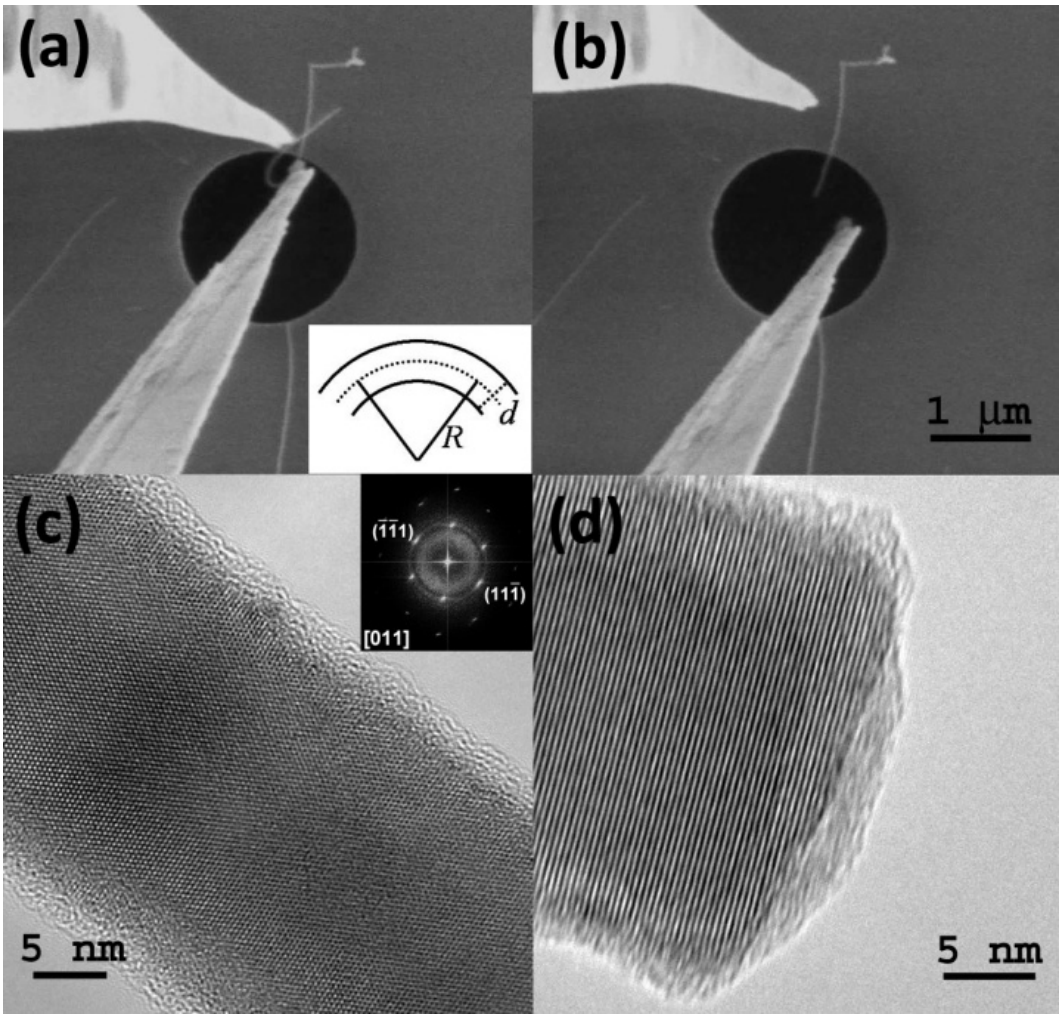

Figure 4.1 (a,b) SEM and (c,d) TEM images of a manipulated Ge nanowire. In (a) and (b), the nanowire is being manipulated with two STM probes. The bent nanowire in (a) has fractured in (b). Inset: Schematic of a bent nanowire. The TEM images in (c) and (d) werre obtained from the fractured Ge nanowire acquired (c) near the substrate (inset: FFT of image) and at the (d) fractured surface.

The flexural strain of the nanowires was determined from the radius of curvature *R*, of the nanowire determined from captured video images. The strain ε_x, at a distance *x* from the neutral axis is related to R as $\varepsilon_x = x/R$. The maximum flexural strain at the point of fracture $\varepsilon_{\max,T}$, occurs at the nanowire surface on the outside of the bend (illustrated in the inset in Figure 4.1a), and relates to the nanowire diameter *d*, and the radius of curvature *R*, as

$$\varepsilon_{\max,T} = \frac{d}{2R} \quad . \tag{4.1}$$

The stress σ_x, in the nanowire at a distance *x* from the neutral axis is proportional to the strain, $\sigma_x = E\varepsilon_x$, where E is the Young's modulus. Bending leads to simultaneous tensile and compressive stresses; however, compressive strengths of ceramic materials are typically 10 to 15 times larger than tensile strengths,[27] and the surface undergoing tensile strain is the expected point of failure. Therefore, the maximum tensile stress at fracture, σ_{bs}, is

$$\sigma_{bs} = E\varepsilon_{\max,T} = E\frac{d}{2R}, \tag{4.2}$$

which is used an approximation to the bending strength.

4.3 RESULTS AND DISCUSSION

The maximum radius of curvature and flexural strain prior to fracture was measured for nanowires with <111> growth direction with diameters ranging from 23 to 97 nm. The strain rate was approximately 10^{-3} s^{-1}, typical for quasi-static strength tests. The maximum radius of curvature and corresponding flexural strain increased

systematically with decreasing nanowire diameter, from 4% to 17% (Figure 4.2). The maximum strain observed in the nanowires was much greater than the 0.04 to 0.06 % measured for bulk Ge.[5]

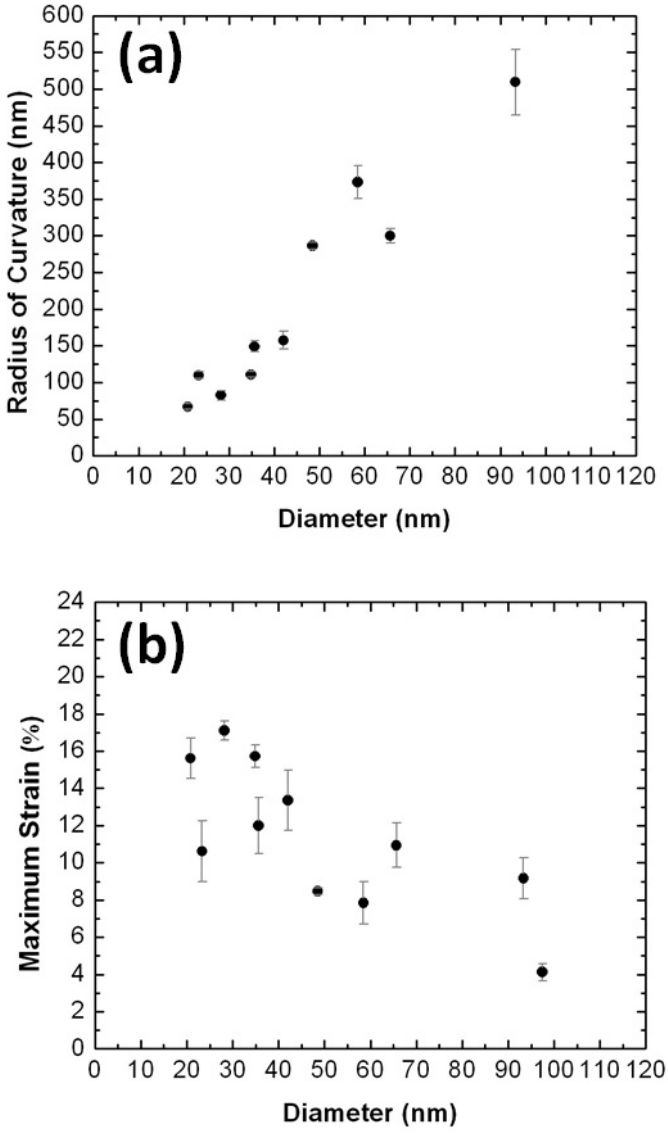

Figure 4.2 Maximum (a) radius of curvature and (b) flexural strain measured for Ge nanowires of varying diameter. All of the nanowires had <111> growth directions, determined from FFTs of HRTEM images (Figure 4.1c inset).

There is a clear trend of increasing bending strength with decreasing diameter. Taking E=106 ± 19 GPa, as previously measured for SFLS-grown Ge nanowires,[16] the bending strengths estimated using Eqn (2) ranged from 4 ± 1 GPa for the largest diameter nanowire to up to 18 ± 4 GPa for the smallest diameters. The bending strengths fall in the range of the theoretical maximum strength of a perfect crystalline solid calculated as $E/2\pi$ (shaded region in Figure 4) and ideal strength calculations from simulations of Ge under tensile loading.[4,28] The bending strength is two to three orders of magnitude greater than bulk Ge. Similar results of size-dependent fracture strengths have been observed for Si nanowires.[29-31] The increase in flexibility and strength with decreased diameter is expected as the number of extended defects present decreases as the volume of the material is reduced.[2]

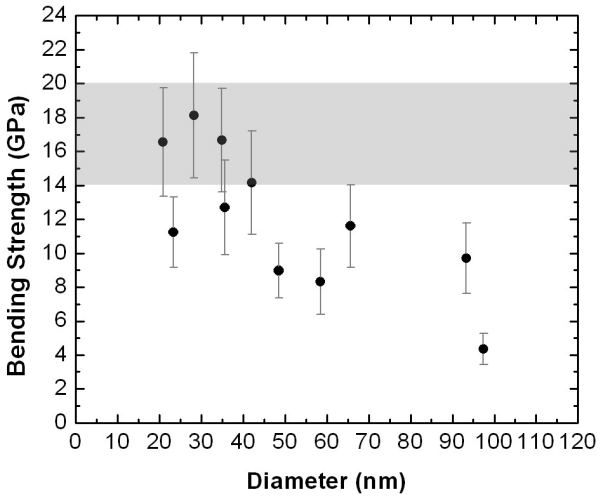

Figure 4.3 Bending strength measured for Ge nanowires of varying diameter. The gray shaded region corresponds to the predicted fracture strength for a perfect Ge crystal.[4,5]

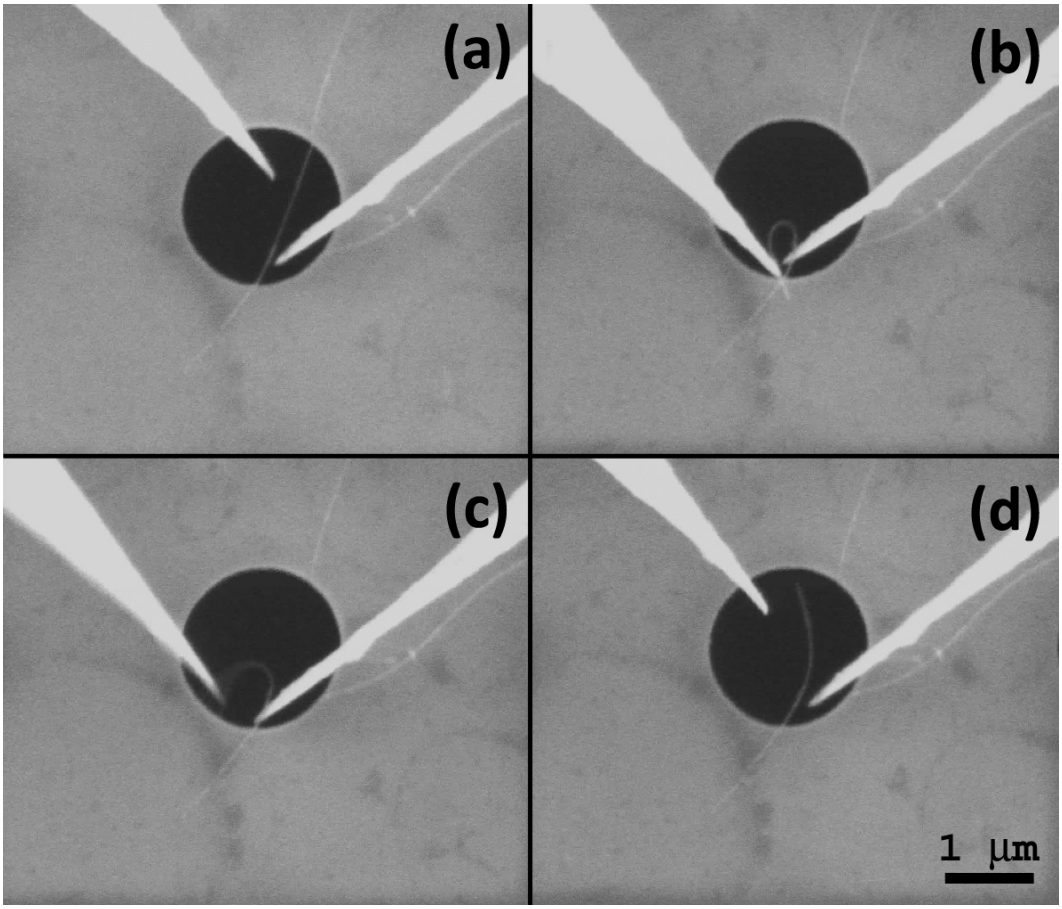

Figure 4.4 Sequence of SEM images of a Ge nanowire being manipulated with two STM probes. From (a) to (b) the nanowire was cut with one of the probes and then bent to a high strain position. The probe has released the nanowire in (c). (d) shows the plastic deformation of the nanowire.

Ge nanowires bent to a position of very high strain and released prior to fracture, were found to exhibit plastic deformation (Figure 4.4). When a nanowire was released, it snapped back quickly, but retained some of its bend (Figure 4.4d). The crystal structure of the nanowire at the position of the bend was examined by TEM to determine the

mechanism involved in plastic deformation of the nanowires. Figure 4.5 shows TEM images of such bent nanowires. At the point of maximum compressive and tensile strain, the nanowire has become amorphous. This observation of amorphization prior to fracture is consistent with the layer of amorphous material that is also observed on fractured surfaces, as in Figure 4.1d.

At the onset of fracture, crack initiation appeared to occur in the amorphous region of the nanowire at the outer strained surface. Experimental and computational studies have shown a transition from crystalline to amorphous structure in strained Si nanowires through an increase in disorder brought about by a large increase in the population of dislocations.[13,32] Indentation studies of crystalline Ge have also shown sudden phase transformations to amorphous Ge (a-Ge) at high loads.[33] The authors of that study speculated that the transformation could occur by the formation of a high-pressure metallic phase followed by quenching to a-Ge as the pressure is released. Considering the large compressive stresses experienced in these specimens, both mechanisms are plausible. However, the detailed mechanism of the mechanically-induced amorphization process requires further study.

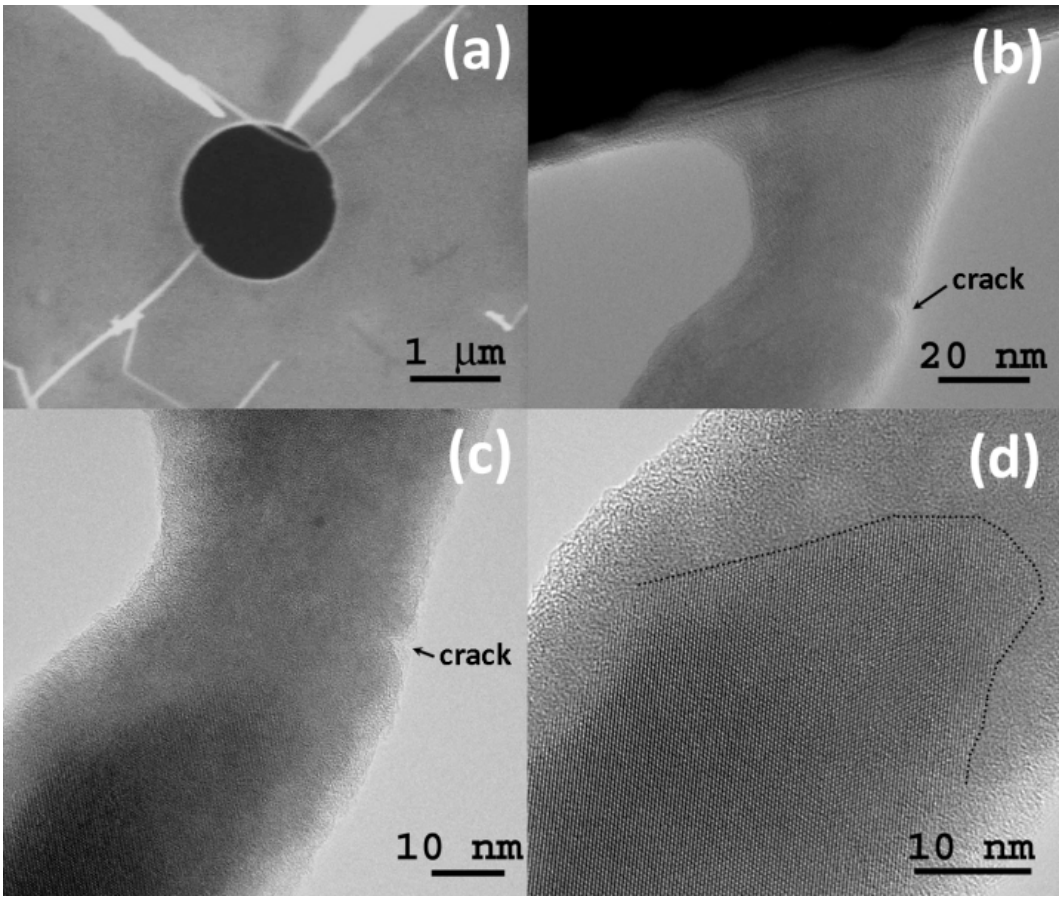

Figure 4.5 (a) SEM image of a cantilevered Ge nanowire bent to a high strain position and pinned to the SiN substrate by Van der Waals forces. (b,c) HRTEM images of the region of highest strain area with the presence of crack formation. The delineation between the diamond-cubic and amorphous phases is clearly shown (dotted line) in HRTEM image (d).

4.4 CONCLUSIONS

The maximum radius of curvature and flexural strain of individual Ge nanowires with diameters between 23 and 97 nm were measured by bending with tungsten probes to the point of fracture. The Ge nanowires are extremely flexible, allowing bending down to a 67 nm radius of curvature for the smallest diameter. Ge nanowires were found to tolerate exceptionally high strains up to 17 %, well in excess of the values of bulk Ge.

The maximum radius of curvature and maximum strain increased with decreasing nanowire diameter expected from a decrease in defects in the reduced volume of the material. The bending strengths of Ge nanowires were determined and found to equal the theoretical fracture strengths of a defect-free, perfect crystalline solid as their diameters were reduced. The corresponding strength-to-weight ratio of the Ge nanowires found in this study is as high as 33.8 kN m/kg, well above many commonly used fiber reinforcements (see Table 4.1). Room temperature plasticity was also observed at extremely high strains. Plastically deformed Ge nanowires exhibited amorphization at the point of maximum strain.

4.5 REFERENCES

(1) Clarke, D. R. In *The Mechanical Properties of Semiconductors*; Faber, K. T., Malloy, K. J., Eds.; Academic Press, Inc.: San Diego, CA, 1992; Vol. 37.

(2) Pearson, G. L.; Read, W. T.; Feldmann, W. L. *Acta. Metall.* **1957**, *5*, 181.

(3) Barrett, C. R.; Nix, W. D.; Tetelman, A. S. *The Principles of Engineering Materials*; Prentice-Hall, Inc.: Englewood Cliffs, NJ, 1973.

(4) Macmillan, N. H. *J. Mater. Sci.* **1972**, *7*, 239.

(5) Claeys, C. *Germanium-Based Technologies: From Materials to Devices*; Elsevier Science: Oxford, 2007.

(6) Davidson, F. M.; Lee, D. C.; Fanfair, D. D.; Korgel, B. A. *J. Phys. Chem. C* **2007**, *111*, 2929.

(7) Hanrath, T.; Korgel, B. A. *J. Am. Chem. Soc.* **2002**, *124*, 1424.

(8) Hanrath, T.; Korgel, B. A. *Adv. Mater.* **2003**, *15*, 437.

(9) Hanrath, T.; Korgel, B. A. *J. Am. Chem. Soc.* **2004**, *126*, 15466.

(10) Ngo, L. T.; Almecija, D.; Sader, J. E.; Daly, B.; Petkov, N.; Holmes, J. D.; Erts, D.; Boland, J. J. *Nano Lett.* **2006**, *6*, 2964.

(11) Hoffmann, S.; Utke, I.; Moser, B.; Michler, J.; Christiansen, S. H.; Schmidt, V.; Senz, S.; Werner, P.; Gosele, U.; Gallif, C. *Nano Lett.* **2006**, *6*, 622.

(12) Zheng, K.; Han, X.; Wang, L.; Zhang, Y.; Yue, Y.; Qin, Y.; Zhang, X.; Zhang, Z. *Nano Lett.* **2009**, *9*, 2471.

(13) Han, X.; Zheng, K.; Zhang, Y. F.; Zhang, X.; Zhang, Z.; Wang, Z. L. *Adv. Mater.* **2007**, *19*, 2112.

(14) Xu, G. In *Dislocations in Solids*; Nabarro, F. R. N., Hirth, J. P., Eds.; North Holland, 2004; Vol. 12, p 83.

(15) Ruoff, R. S.; Qian, D.; Liu, W. K. *C. R. Physique* **2003**, *4*, 993-1008.

(16) Smith, D. A.; Holmberg, V. C.; Lee, D. C.; Korgel, B. A. *J. Phys. Chem. C* **2008**, *112*, 10725.

(17) Kumar, S.; Wang, Y. In *Composites Engineering Handbook*; Mallick, P. K., Ed.; Marcel Dekker, Inc.: New York, 1997.

(18) Ruoff, R. S.; Lorents, D. C. *Carbon* **1995**, *33*, 925.

(19) Law, M.; Goldberger, J.; Yang, P. *Annu. Rev. Mater. Res.* **2004**, *34*, 83.

(20) Wong, E. W.; Sheehan, P. E.; Lieber, C. M. *Science* **1997**, *277*, 1971.

(21) Lee, B.; Rudd, R. E. *Phys. Rev. B* **2007**, *75*, 041305.

(22) He, R.; Yang, P. *Nature* **2006**, *1*, 42.

(23) Wu, B.; Heidelberg, A.; Boland, J. J. *Nature* **2005**, *4*, 525.

(24) Hsin, C. L.; Mai, W.; Gu, Y.; Gao, Y.; Huang, C. T.; Liu, Y.; Chen, L. J.; Wang, Z. L. *Adv. Mater.* **2008**, *20*, 1.

(25) Chen, X.; Zhang, S.; Wagner, G. J.; Ding, W.; Ruoff, R. S. *J. Appl. Phys.* **2004**, *95*, 4823.

(26) Mechanical measurements were performed using a Zyvex S100 nanomanipulation system inside of a FEI Strata 235 dual beam SEM/FIB system. Tungsten probes were made by electrochemically etching tungsten wire (Goodfellow, 0.25 mm, 99.95% purity) in 2 M KOH at a bias of 4 V. The nanomanipulator was used to

bend nanowires until fracture or to a high strain position. Video of specimen manipulation was obtained by splitting the monitor signal and capturing on a separate computer using a VGA2USB VGA capture device from epiphan systems inc. The video was recorded at a frame rate faster than the SEM scan rate of 0.34 seconds.

(27) Roesler, J.; Harders, H.; Baeker, M. *Mechanical Behaviour of Engineering Materials*; Springer: New York, 2007.

(28) Roundy, D.; Cohen, M. L. *Phys. Rev. B* **2001**, *64*, 212103.

(29) Tabib-Azar, M.; Nassirou, M.; Wang, R. *Appl. Phys. Lett.* **2005**, *87*, 113102.

(30) Gordon, M. J.; Baron, T.; Dhalluin, F.; Gentile, P.; Ferret, P. *Nano Lett.* **2009**, *9*, 525.

(31) Namazu, T.; Isono, Y.; Tanaka, T. *J. Microelectromech. S.* **2000**, *9*, 450.

(32) Menon, M.; Srivastava, D.; Ponomareva, I.; Chernozatonski, L. A. *Phys. Rev. B* **2004**, *70*, 125313.

(33) Oliver, D. J.; Bradby, J. E.; Williams, J. S. *J. Appl. Phys.* **2007**, *101*, 043524.

Chapter 5: Optical Properties of Germanium Nanowires

5.1 INTRODUCTION

Germanium (Ge) has a relatively low optical dispersion and high index of refraction, which has led to its use in a host of optical and optoelectronic applications.[1] Therefore, Ge nanowires are an excellent choice for studying nanoscale optical properties and devices. Ordered arrays of Ge nanowires have recently been fabricated for use as photoresistors.[2] Also, Cao et al. demonstrated that resonant optical modes led to unexpected changes in the optical absorption of single Ge nanowire devices, which varied dramatically with diameter and orientation.[3] In addition to the novel optical properties of semiconductor nanowires, these materials often possess enhanced mechanical properties due to the reduced presence of defects. In chapters 3 and 4, it was shown that Ge nanowires also exhibit extraordinary mechanical properties such as extremely high flexibility and strength, with strength-to-weight ratios exceeding high strength steel. Therefore, it is interesting to consider these materials as multifunctional structural fibers in composites.

In this chapter, two methods of producing well dispersed Ge nanowire samples by fabricating nanowire-polymer films and by creating solutions of PEGylated nanowires are demonstrated. The nanowires exhibit optical absorbance spectra with features that differ from bulk Ge. Ge nanowire spectra and the internal electric field intensity within the nanowire were simulated using a numerical solution of Maxwell's equations, the discrete dipole approximation (DDA), to assist in determining contributions from

individual wires.[4] The calculated spectra match the experimental measurements quite well, providing evidence that resonant optical modes within the nanowires are largely responsible for the difference in optical properties. Further, the model demonstrates the potential to tune the optical properties of the nanowires by manipulating their size and orientation.

5.2 EXPERIMENTAL DETAILS

5.2.1 Composite Fabrication

Germanium (Ge) nanowires were synthesized by the supercritical fluid-liquid-solid (SFLS) method described in Chapter 2. Composite films were fabricated by mixing the dodecene-passivated Ge nanowires with Kraton SBS triblock copolymer (D1102K) in toluene at the desired weight percents. The solutions were sonicated for 5 minutes and deposited into a stainless steel mold. The solutions were allowed to evaporate overnight and then placed in a vacuum oven (Fisher Isotemp 281A) at room temperature and a vacuum of approximately 729 Torr for one hour to remove any residual solvent. Round films 4 cm in diameter and approximately 100 μm thick were fabricated. The combination of surface passivation and the high viscosity due to the addition of the SBS copolymer produced well dispersed films with minimal aggregation.

5.2.2 Absorbance Measurements

Absorbance spectra were obtained in transmission mode (Varian Cary 500 UV-Vis Spectraphotometer) by mounting the composite films over a 10 x 20 mm aperture. Spectra were taken between wavelengths of 300 and 3000 nm.

5.3 SIMULATIONS

For arbitrary shapes like core-shell particles, rods, or ensembles, the DDA has been used to successfully model absorption and scattering behavior of nanoparticles and interstellar dust grains.[5] The details of the DDA method have been published in several works.[4,6] The method approximates a particle by an array of point dipoles which is valid as long as the spacing between dipoles is small compared to the wavelength of light. The dipoles are arrange on a cubic grid located at a position $\vec{r}_j$ with a complex polarizability $\tilde{\alpha}_j$. The polarization of each dipole is

$$\vec{P}_j = \tilde{\alpha}_j \vec{E}_{loc,j}, \tag{5.1}$$

where $\vec{E}_{loc,j}$ is the local electric field at point $\vec{r}_j$ due to the incident electric field $\vec{E}_{inc,j}$ and the electric field emitted by all other dipoles in the system, $\vec{E}_{dipole,j}$. The electric field at position j due to all neighboring dipoles can be expressed as

$$\vec{E}_{dipole,j} = -\sum_{k \neq j} \tilde{A}_{jk} \vec{P}_k, \tag{5.2}$$

where

$$\tilde{A}_{jk} = \frac{e^{i\kappa r_{jk}}}{r_{jk}} \left[\kappa^2 \left(\hat{r}_{jk} \hat{r}_{jk} - \tilde{1}_3 \right) + \frac{i\kappa r_{jk} - 1}{r_{jk}^2} \left(3\hat{r}_{jk} \hat{r}_{jk} - \tilde{1}_3 \right) \right] \tag{5.3}$$

and $\kappa = \omega / c$. r_{jk} is the distance from dipole j to dipole k, $\hat{r}_{jk}$ is the unit vector in the r_{jk} direction, and $\tilde{1}_3$ is the 3x3 identity matrix. For *N* dipoles, the polarizations of each dipole $\vec{P}_j$ can be found by solving the system of 3*N* complex linear equations described by

$$\sum_{k=1}^{N} \tilde{A}_{jk} \vec{P}_k = \vec{E}_{inc,j}, \tag{5.4}$$

where

$$\tilde{A}_{jj} = \tilde{\alpha}_j^{-1}. \tag{5.5}$$

The polarization of each dipole is related to the complex dielectric constant $\tilde{\varepsilon}_j$ of the material through the use of the Claussius-Mossotti relation

$$\tilde{\alpha}_j = a^3 \frac{\tilde{\varepsilon}_j - \varepsilon_{hst}}{\tilde{\varepsilon}_j - 2\varepsilon_{hst}}, \tag{5.6}$$

where a is the effective radius of the dipole and ε_{hst} is the dielectric constant of the host material. In our simulations, dielectric data from the literature is used. The radiative correction established by Draine[4,6]

$$\tilde{\alpha}_{cor,j} = \frac{\tilde{\alpha}_j}{1 - i\frac{2k^3}{3}\tilde{\alpha}_j} \tag{5.7}$$

is adopted in our calculations, which corrects the polarizability for a finite dipole. Figure 5.1 illustrates the nanowire model used for simulations in this study, which consists of a 2 x 2 dipole cross section with the number of dipoles along the long axis determined by the desired length. The diameter of the nanowire is defined from the outer edges of the dipoles across the diagonal of the cross section

$$D = 2a + \sqrt{2}d \ , \tag{5.8}$$

where a is the radius of the dipole and d is the dipole spacing. Utilizing the method proposed by Podolskiy et al.,[7] multipolar corrections to the depolarization factor are taken into account by defining

$$\frac{a}{d} \approx 1.688 . \tag{5.9}$$

Once a solution is found for the polarizations of the *N* dipoles in the system, the extinction C_{ext} and absorption C_{abs} cross sections can be calculated by

$$C_{ext} = \frac{4\pi k}{|E_0|^2} \sum_{j=1}^{N} \mathrm{Im}\left(\vec{E}_{inc,j} * \cdot \vec{P}_j\right) \tag{5.10}$$

and

$$C_{abs} = \frac{4\pi k}{|E_0|^2} \sum_{j=1}^{N} \left\{ \mathrm{Im}\left[\vec{P}_j \cdot \left(\tilde{\alpha}_j^{-1}\right) * \vec{P}_j *\right] - \frac{2}{3} k^3 \left(\vec{P}_j \cdot \vec{P}_j *\right) \right\}, \tag{5.11}$$

respectively. The total electric field at each dipole can be acquired by using equation (5.1) with the calculated polarizations.

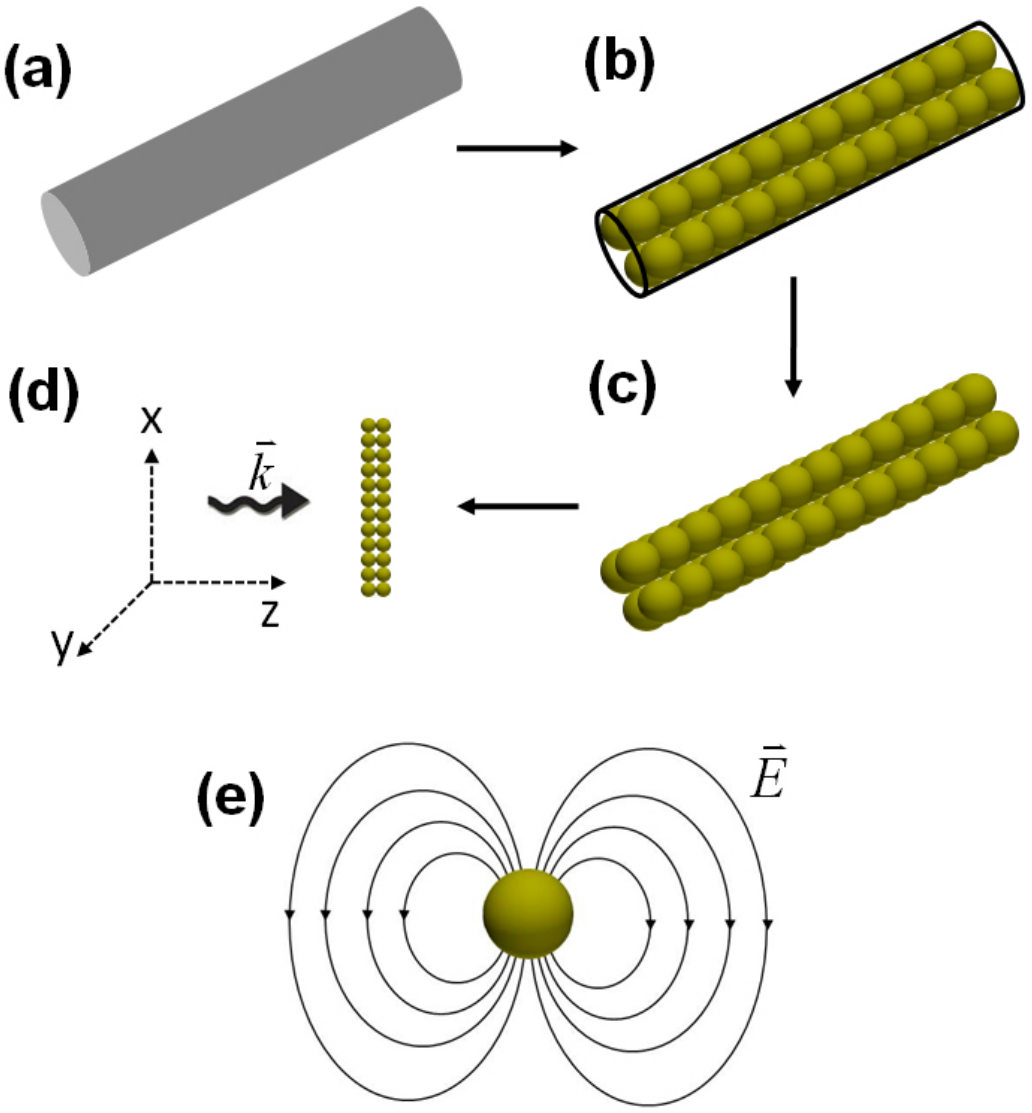

Figure 5.1. Schematic of the model used for the discrete dipole approximation calculation. The nanowire (a) is approximated by filling the volume with an array of dipoles with a 2 x 2 dipole cross section (b), (c). (d) Incident light is applied to the collection of dipoles with a particular polarization with respect to the model. (e) Illustration of the electric field lines emanating from each dipole. The total electric field at a particular dipole is a sum of the incident electric field and the field from all other dipoles in the model.

5.4 RESULTS AND DISCUSSION

5.4.1 Absorbance Measurements

Figure 5.2a shows the absorbance spectra of Kraton-Ge nanowire composites with two different nanowire loadings, of 0.3, and 0.7 weight percent nanowires compared to the pure polymer. The absorbance spectra for the PEGylated Ge nanowires prepared as described in chapter 2 are shown in Figure 5.2b. The polymer-Ge composites show a series of similar peaks beyond 1600 nm wavelengths which correspond to the Kraton polymer. An absorption peak near 600 nm and a small shoulder at slightly higher energy is present in both the Ge nanowire composites and PEGylated Ge nanowires. In addition, the dependence of absorbance as a function of wavelength at energies above the band edge (approximately 1850 nm) is significantly different than what is expected for Ge. Also, the samples begin absorbing slightly below the band gap energy.

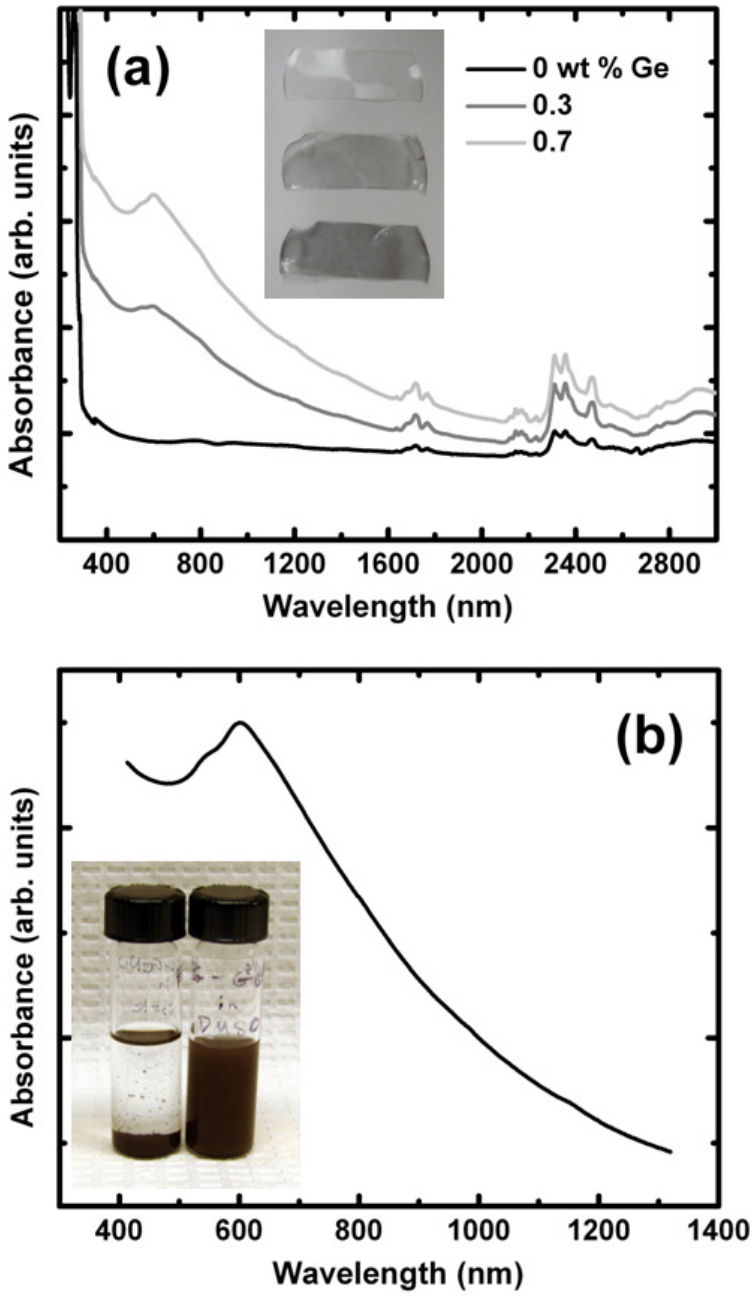

Figure 5.2 (a) Absorption spectra of 100 μm thick Kraton and Kraton-Ge nanowire composites with two different Ge nanowire loadings. Inset: Photograph of the Kraton-Ge nanowire composites. (b) Absorption spectra of PEGylated Ge nanowires. Inset: Photograph of the Ge nanowires-DMF solution before (left) and after (right) PEGylation.

5.4.2 Simulations

Figure 5.3 shows the simulated extinction cross section spectra for a single 2 μm long Ge nanowire with diameters varying from 10 to 90 nm. The spectra show high sensitivity to the polarization of the incident electric field. Polarization anisotropy of absorption and emission in semiconductor nanowires has been observed in several cases and could certainly play a role in our system.[8,9] For polarizations perpendicular to the long axis of the nanowire (Figure 5.3a), the spectra show a dramatic decrease in extinction at approximately 500 nm wavelengths at small diameters. A peak at 600 nm is observed in larger diameter wires qualitatively similar to the experimental peaks observed in Figure 5.2. The simulations for the incident electric field aligned along the long axis of the nanowire (Figure 5.3b) exhibit much more complex spectra which change dramatically depending on nanowire diameter. In our system of randomly distributed nanowires and randomly polarized light, we expect an averaging of these effects. However, the possibility of aligning nanowires in composite films could be utilized to enhance the behavior of a particular orientation.[10]

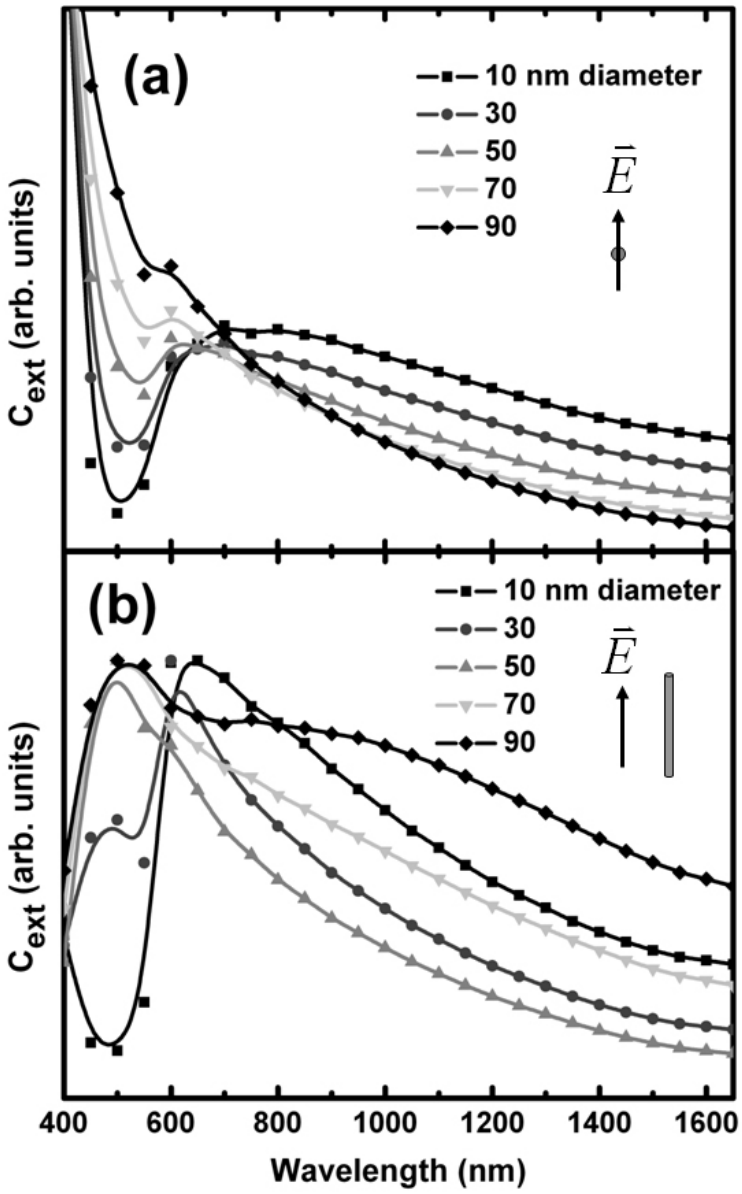

Figure 5.3 Normalized extinction cross section of Ge nanowires with varying diameter for incident light polarizations (a) perpendicular and (b) parallel to the nanowire axis.

The Ge nanowire-polymer composites have randomly oriented nanowires distributed in the polymer. The nanowire model is tilted 45° off the x-, y-, and z-axis

with an incident electric field applied in along the x-direction (inset Figure 5.4a) so that the electric field vector is evenly distributed along the three dimensions of the nanowire and is used to approximate the general case of randomly polarized light impinging upon the sample on average. Figure 5.4a shows the results in this case for a 30 nm diameter nanowire with a length of 2 μm, a typical average nanowire size for our synthesis.[11,12] By looking separately at the extinction, absorption, and scattering cross-sections, the peak observed in our data and the simulations at 600 nm appears to be primarily due to absorption. Figure 5.4b displays the electric field intensity distribution along the length of the nanowire for incident wavelengths between 400 and 800 nm. While the current model doesn't possess the resolution for detailed internal electric field intensity within the nanowire, an enhancement of the field along the middle portion of the nanowire is observed in the nanowires for this orientation and size. Larger relative electric field intensities between 500 nm and 600 nm are observed, corresponding to the range where we measured peaks in our experimental spectra. Therefore, individual nanowires may be acting effectively as light trapping sources. The peak in the simulations at 500 nm wavelengths is primarily attributed to scattering. This scattering peak is not present in our experimental data. However, the scattering in our system should possess much more complex behavior from the ensemble of nanowires, as opposed to a single wire, and is discussed in more detail below.

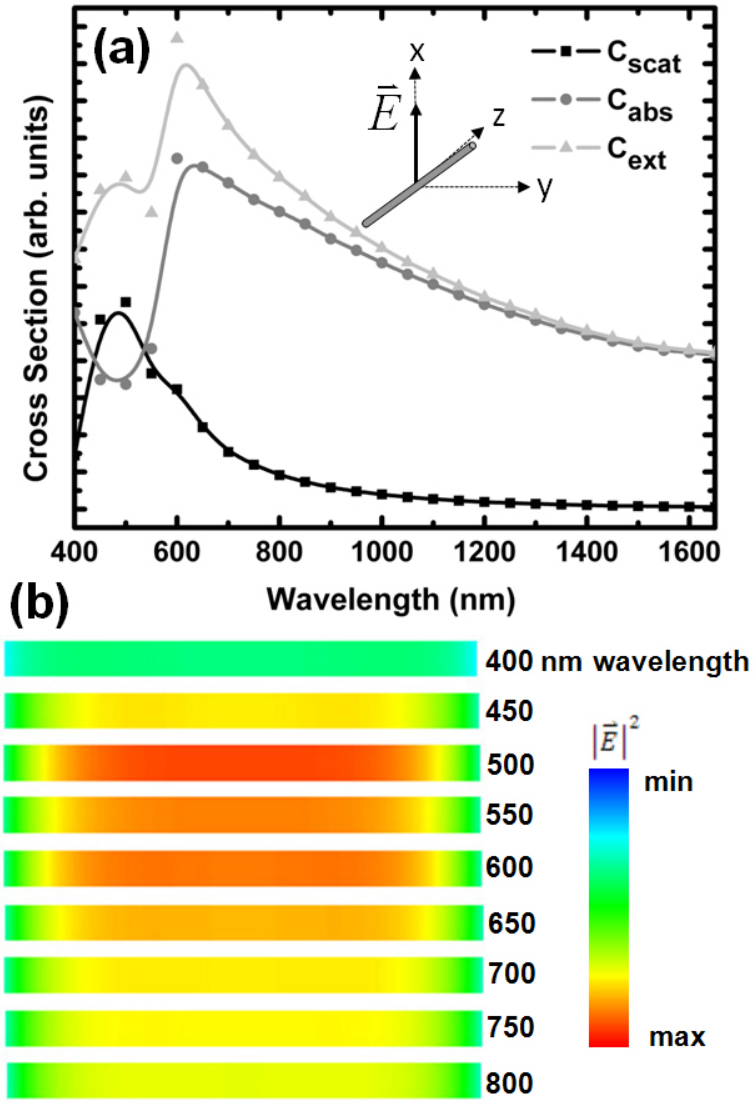

Figure 5.4 (a) Scattering, absorption, and extinction cross section of a 30 nm germanium nanowire with a length of 2 μm. Inset: Schematic showing the length of the nanowire is tilted 45° from the x-, y-, and z-axis and the incident electric field is in the x-direction. (b) Internal electric field intensity for incident wavelengths between 400 and 800 nm.

The calculated extinction spectra for the 30 nm diameter wire is compared to the experimental data from the Ge nanowire-polymer composite, PEGylated Ge nanowires, and bulk Ge in Figure 5.5. The slope with increasing energy above the band edge of 0.67

eV is markedly different from bulk Ge, exhibiting linear behavior. Light trapping from the random orientation of nanowires in the film and solution can explain the difference in slope from bulk Ge. The random arrangement causes a lengthening of the path of light rays in the material, increasing the interaction with nanowires and further increasing absorption.[13-16] In addition, absorption appears to occur slightly below the band gap energy. This likely results from interference from the Kraton polymer, but could also result from the presence of surface states. In a previous study, the presence of surface states on the Ge nanowires were found which greatly affected their electronic properties.[17] Surface states have also been found to attribute to infrared light trapping leading to enhanced absorption below the bandgap in silicon nanowires.[16] While the model does match qualitatively to the experimental data, there is some deviation at higher energies. This deviation may be a result of the collective behavior of the nanowires in this energy range.

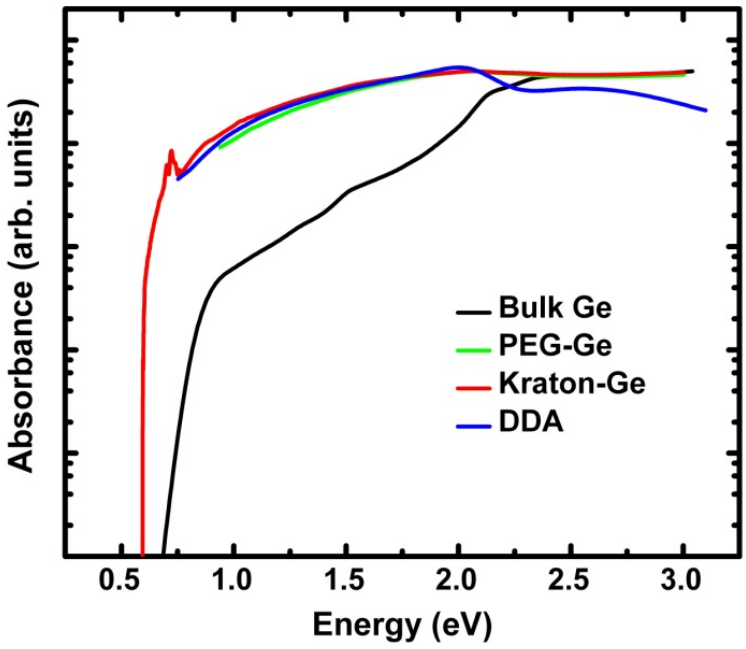

Figure 5.5 Comparison of the normalized absorption spectra of bulk Ge, PEGylated Ge nanowires, Kraton-Ge nanowire composite, and DDA simulation of a 30 nm diameter nanowire with a length of 2 μm.

5.5 CONCLUSIONS

Ge nanowire-polymer composites and well-dispersed PEGylated Ge nanowires in solution were used to measure the optical properties of the nanowires. The absorbance spectra of the nanowires were found to have markedly different behavior from their bulk counterpart. A coupled dipole method, the DDA, was used to explore the presence of peaks in the absorbance spectra and the difference in the material's dependence on incident light energy by using a simple model of an individual Ge nanowire. Simulations showed extinction spectra that depend significantly on the size of the nanowires and the incident electric field polarization. Modeling of an average size nanowire with an approximation to incident randomly polarized light impinging on randomly oriented

nanowires displayed qualitative agreement with the experimental spectra. The major peak at 600 nm wavelengths can be attributed to a resonant optical mode in the individual nanowires leading to enhanced absorption by acting as a subwavelength optical trap. The difference in energy dependence of the measured absorbance spectra is likely caused by a combination of surface state-induce trapping and enhanced absorption through increased interparticle scattering within the films and solution. The simulation results demonstrate the potential to engineer the absorption and light trapping behavior of semiconductor nanowire devices and films by tuning their size-, shape-, and orientation-dependent optical interactions.

5.6 REFERENCES

(1) Claeys, C. *Germanium-Based Technologies: From Materials to Devices*; Elsevier Science: Oxford, 2007.

(2) Polyakov, B.; Daly, B.; Prikulis, J.; Lisauskas, V.; Vengalis, B.; Morris, M. A.; Holmes, J. D.; Erts, D. *Adv. Mater.* **2006**, *18*, 1812.

(3) Cao, L.; White, J. S.; Park, J. S.; Schuller, J. A.; Clemens, B. M.; Brongersma, M. L. *Nat. Mater.* **2009**, *8*, 643.

(4) Draine, B. T. *Astrophysical J.* **1988**, *333*, 848.

(5) Yurkin, M. A.; Hoekstra, A. G. *J. Quant. Spectrosc. Ra.* **2007**, *106*, 558.

(6) Draine, B. T.; Flatau, P. J. *J. Opt. Soc. Am. A* **1994**, *11*, 1491.

(7) Podolskiy, V. A. *J. Nonlinear Opt. Phys.* **2002**, *11*, 65.

(8) Agarwal, R.; Lieber, C. M. *Appl. Phys. A-Mater.* **2006**, *85*, 209-215.

(9) Wang, J.; Gudiksen, M. S.; Duan, X.; Cui, Y.; Lieber, C. M. *Science* **2001**, *293*, 1455.

(10) Bashouti, M.; Salalha, W.; Brumer, M.; Zussman, E.; Lifshitz, E. *ChemPhysChem* **2006**, *7*, 102.

(11) Hanrath, T.; Korgel, B. A. *J. Am. Chem. Soc.* **2002**, *124*, 1424.

(12) Hanrath, T.; Korgel, B. A. *Adv. Mater.* **2003**, *15*, 437.

(13) Hu, L.; Chen, G. *Nano Lett.* **2007**, *7*, 3249.

(14) Muskens, O. L.; Diedenhofen, S. L.; Weert, M. H. M.; Borgstrom, M. T.; Bakkers, E. P. A. M.; Rivas, J. G. *Adv. Funct. Mater.* **2008**, *18*, 1039.

(15) Muskens, O. L.; Rivas, J. G.; Algra, R. E.; Bakkers, E. P. A. M.; Lagendijk, A. *Nano Lett.* **2008**, *8*, 2638.

(16) Tsakalakos, L.; Balch, J.; Fronheiser, J.; Shih, M. Y.; LeBoeuf, S. F.; Pietrzykowski, M.; Codella, P. J.; Korevaar, B. A.; Sulima, O.; Rand, J.; Davuluru, A.; Rapol, U. *J. Nanophotonics* **2007**, *1*, 013552.

(17) Hanrath, T.; Korgel, B. A. *J. Phys. Chem. B* **2005**, *109*, 5518.

CHAPTER 6: GERMANIUM NANOWIRE NONWOVEN FABRIC

6.1 INTRODUCTION

Great progress has been made in the assembly of individual and multiple nanowires into device structures through techniques such as Langmuir-Blodgett transfer, dielectrophoresis, and self-assembly.[1-3] However, huge challenges still remain for scaled up fabrication of these device structures using these techniques. Recently, there has been enthusiasm over the development of macroscopic sheets of mechanically stable free-standing films of carbon nanotube (CNT) paper or fabric (or Buckypaper).[4-7] This research has produced thin films of randomly and aligned CNTs with potential applications as supercapacitors, hydrogen storage materials, anode materials in lithium ion batteries, actuators, and sensors. With the development of scalable synthetic methods for producing semiconductor nanowires, this approach is now feasible for these materials. This opens up the opportunity to explore fabrics with properties only achievable with semiconductor materials.

In this chapter, vacuum filtration is used to produce sheets of a nonwoven bendable fabric composed of germanium (Ge) nanowires of different thicknesses and a cursory exploration of their use as photoresistors is explored.

6.2 EXPERIMENTAL DETAILS

6.2.1 Nanofabric Fabrication

Ge nanowires are synthesized using the gold-nanocrystal seeded super critical fluid-liquid-solid (SFLS) method inside of titanium reactor followed by in situ surface

passivation with dodecene using the methods described in Chapter 2. A dilute dispersion of the nanowires in toluene (~ 0.1 mg/mL) was created. Any small bundles of nanowires in the solution are broken up using a combination of sonication for 5 minutes (Cole-Parmer 8891) followed by injection through a syringe with a small diameter needle (20 G). A simple vacuum filtration setup (Figure 6.1a) is used to produce the nanowire fabric. The setup consists of a funnel attached to an aspirator with a porous alumina membrane placed in the bottom of the funnel to collect the nanowires. Depending on the desired fabric thickness, a particular volume of the nanowire dispersion is poured into the funnel under a light vacuum. After the nanowires have collected on the filter, ethanol is poured in the funnel to remove any excess ligands.

6.2.2 Electronic and Photoconductivity Measurements

A small portion of the Ge fabric was scissor cut and applied to gold interdigitated array (IDA) electrodes on a glass substrate. The IDA was fabricated using standard photolithography techniques. The IDA consisted of 100 finger electrodes, 5 μm spaced, over a 1 mm area. The piece of Ge fabric was attached to the IDA by placing a 5 μL drop of toluene on the fabric and dried for 1 hour under vacuum (~ 700 Torr).

6.3 Results and Discussion

Figure 6.1b shows the alumina membrane after filtration with the Ge nanowires collected on the top. After the fabric has air dried for approximately 1 hour, it can be peeled from the filter (Figure 6.1c).

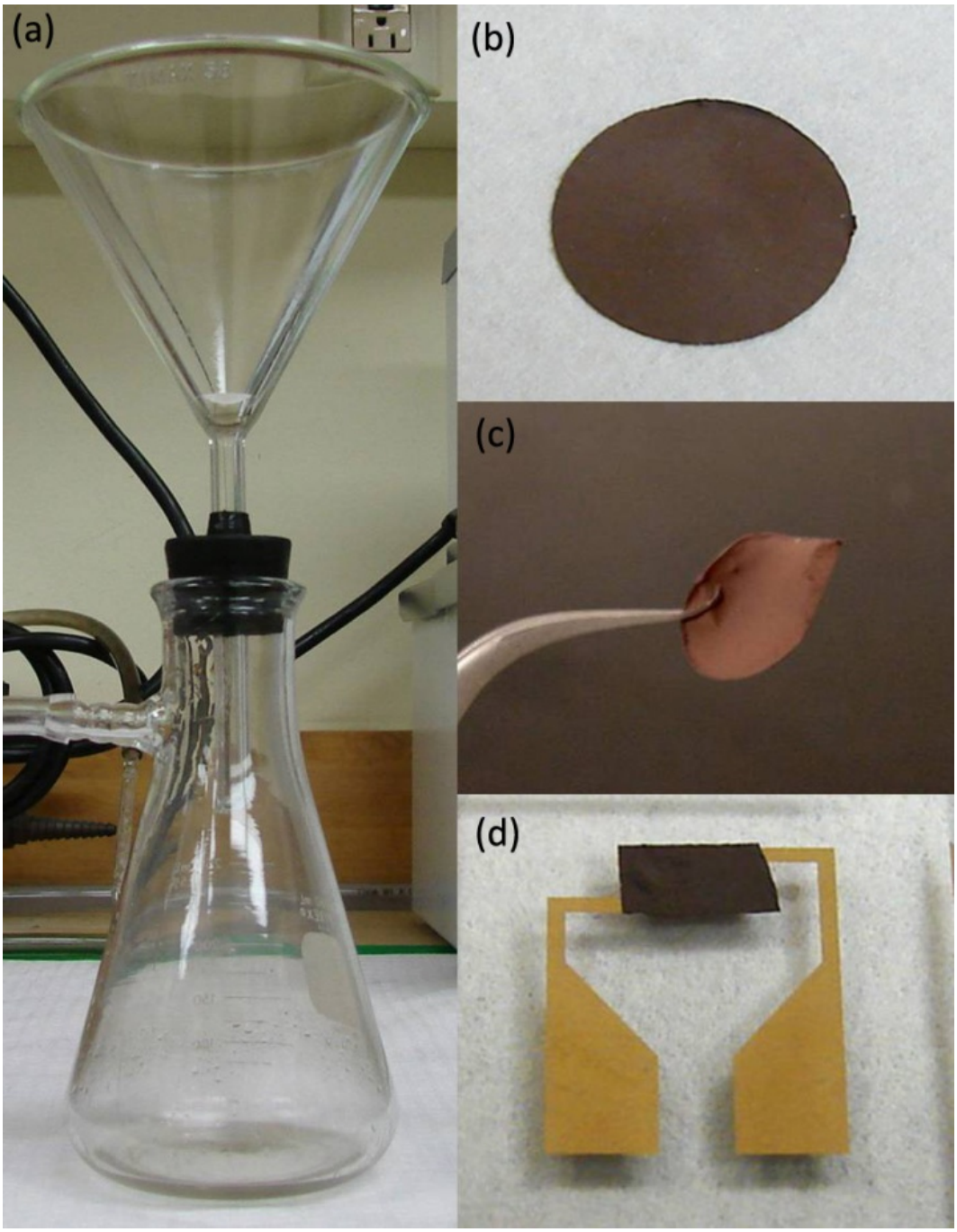

Figure 6.1 The Ge nanowire fabric is made using a simple (a) vacuum filtration setup. (b) Image of Ge nanowires collected on an alumina filter. (c) After the fabric dries, it is peeled away from the membrane. (d) The fabric can then be cut into different shapes with scissors and applied to a device such as the Au IDA shown here.

Figure 6.2 shows representative scanning electron microscope (SEM) images of the nanowire fabric. These images show the difference in texture of the bottom and top surfaces of the fabric. The side of the fabric which was initially facing the filter has a much smoother glossy texture, while the top surface has a rougher surface. This is a result of the smooth surface of the alumina membrane and some aggregation of nanowires into bundles as the fabric becomes thicker. The filtering process becomes slower as the nanowires collect on the membrane, therefore larger bundles are able to begin to precipitate out before the toluene has passed through the filter. This difference in surface roughness could be reduced or enhanced through a combination of better control of dispersibility and a more sophisticated filtration setup with precise control of vacuum pressure.

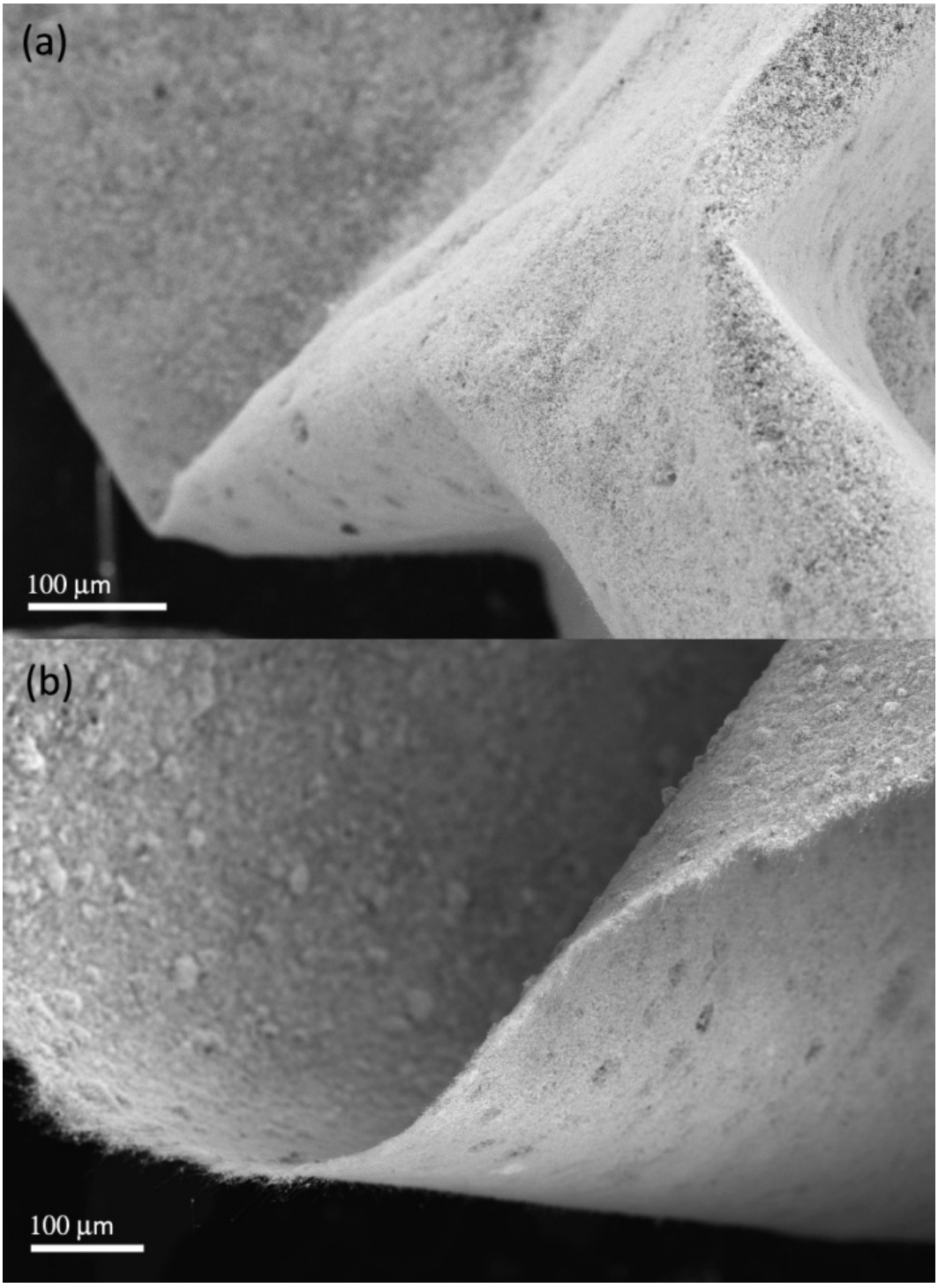

Figure 6.2 (a), (b) Low resolution SEM images of the Ge nanowire fabric. Image (b) clearly shows the difference in texture of the top and bottow surfaces.

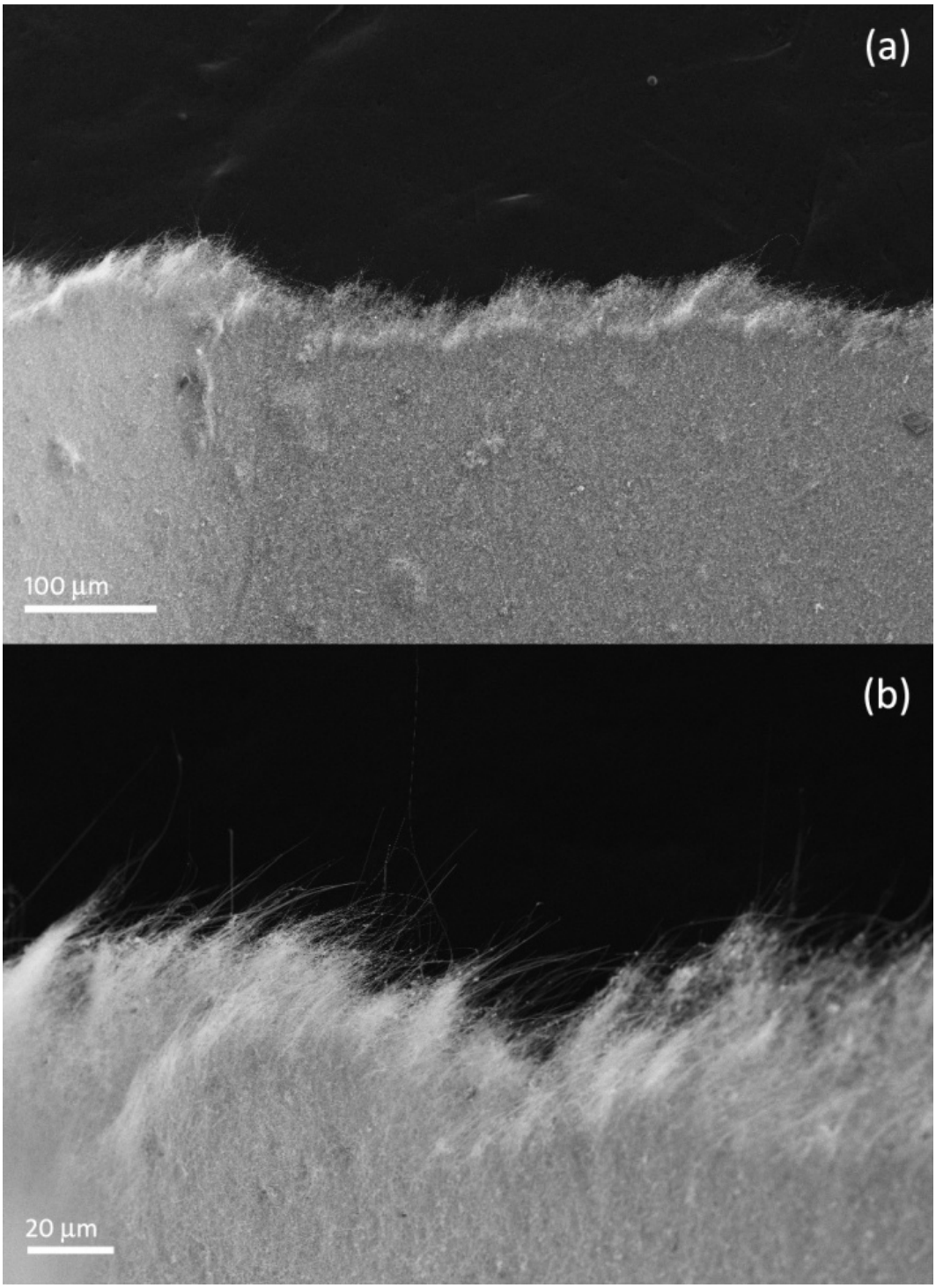

Figure 6.3 (a) Low and (b) high resolution SEM images of a section of torn Ge nanowire fabric.

Figure 4a shows SEM image of the edge of a thin piece of Ge fabric approximately 7.5 μm thick. Figure 6.4b shows a well defined edge of thicker, approximately 25 μm thick, paper after cutting with scissors. The thin fabric was produce by filtration of approximately 0.5 mg of Ge nanowires, while the thicker fabric was made with 1.25 mg. Because of the increase in pressure of the vacuum filtration setup as the fabric becomes thicker, an alternate method of controlling thickness could be attained by monitoring this pressure as the nanowire solution is added. From the measured mass and dimensions of the nanowire fabric the density of the fabric is calculated to be approximately 1 % of the density of bulk Ge, containing roughly 10 % Ge nanowires and 90 % void space by volume.

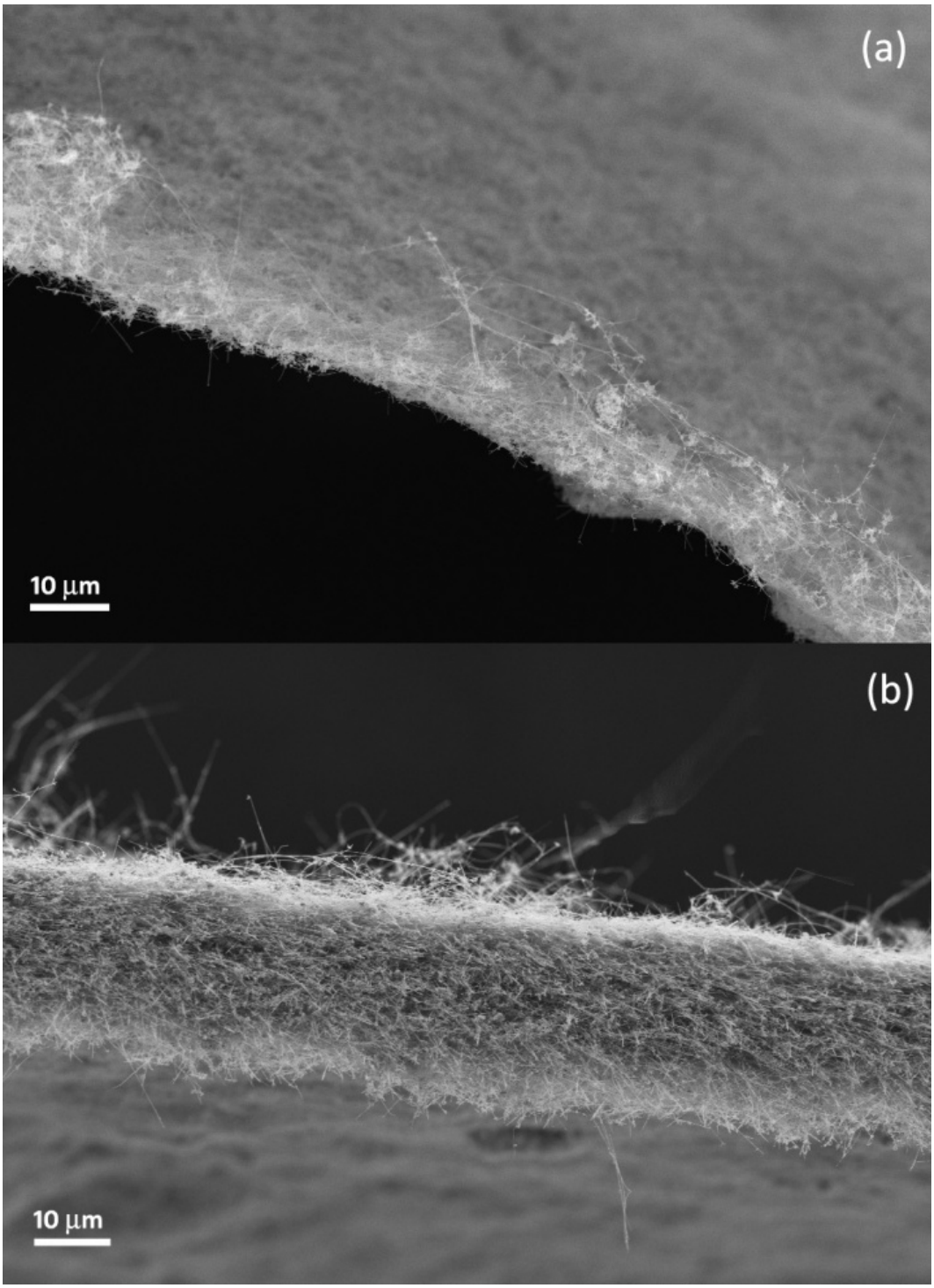

Figure 6.4 SEM images of the edges of (a) thin and (b) thick Ge nanowire paper.

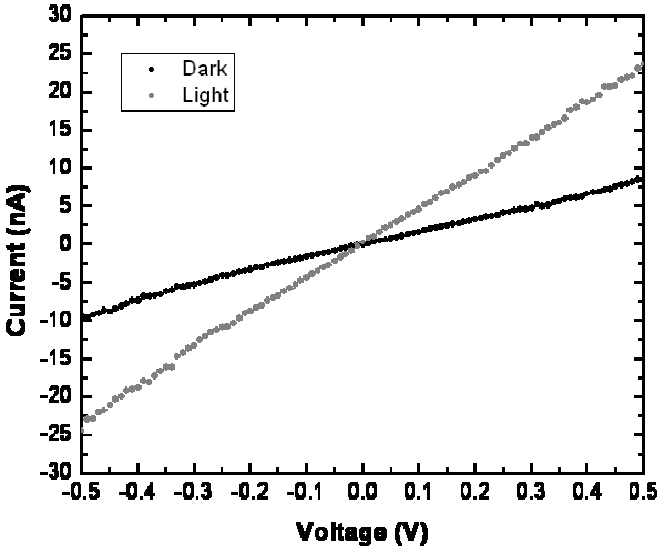

Figure 6.5 IV curves of the Ge paper on Au IDA shown in Figure 1d take in dark and light (1 sun, AM 1.5 G) conditions.

Figure 6.5 displays the Current-Voltage (IV) curves of the 25 mm thick paper attached to the gold IDA for dark and light (1 sun, AM 1.5 G) conditions. The data show an increase in conductivity upon light exposure.

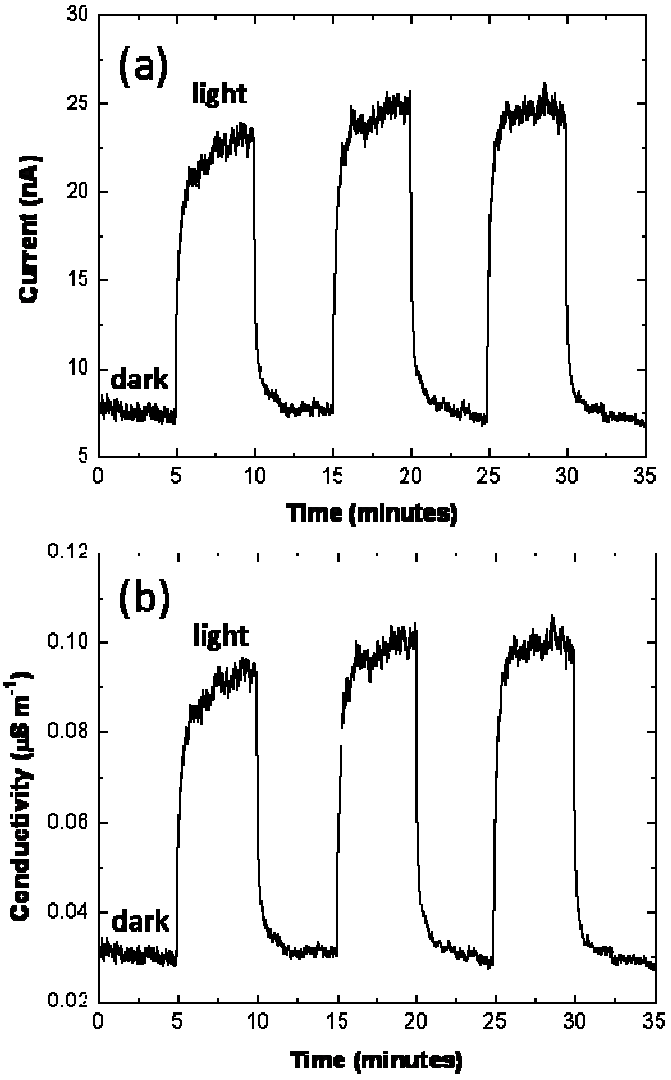

Figure 6.6 (a) Current and (b) conductivity of a Ge fabric device taken in alternating dark and light conditions.

Data was also taken in light and dark conditions over three cycles with each light and dark segment taken over a 5 minute interval at 0.5 V. Figure 6.6a shows the change in current and Figure 6.6b shows the change in conductivity demonstrating an

approximate 200 % increase in conductivity. The graphs show responses over two time scales for the increase and decrease in current. The initial response is a result of photoactive processes occurring in the nanowire fabric, while the second is likely a result of thermal processes.[8]

6.4 CONCLUSIONS

Ge nanowire fabric of varying thickness have been made by vacuum filtration of different amounts of nanowires dispersed in an organic solvent. The fabric formed is 1 % of the density of bulk Ge and contains 10 % wires and 90 % void space by volume. SEM images of the top and bottom sides of the fabric display a smooth bottom and rough top. The fabric was mechanically stable enough to be handled and manipulated for testing. Additionally, the fabric was found to be photoconductive with a 200 % increase in conductivity at 0.5 Volts under 1 sun, AM 1.5 G light conditions. The development of semiconductor nanowire sheets opens up the study of a new class of material.

6.5 REFERENCES

(1) Smith, P. A.; Nordquist, C. D.; Jackson, T. N.; Mayer, T. S.; Marin, B. R. *Appl. Phys. Lett.* **2000**, *77*, 1399.

(2) Whang, D.; Jin, S.; Wu, Y.; Lieber, C. M. *Nano Lett.* **2003**, *3*, 1255.

(3) Yang, P. *Nature* **2003**, *425*, 243.

(4) Bahr, J. L.; Yang, J.; Kosynkin, D. V.; Bronikowski, M. J.; Smalley, R. E.; Tour, J. M. *J. Am. Chem. Soc.* **2001**, *123*, 6536.

(5) Endo, M.; Muramatsu, H.; Hayashi, T.; Kim, Y. A.; Terrones, M.; Dresselhaus, M. S. *Nature* **2005**, *433*, 476.

(6) Gonnet, P.; Liang, Z.; Choi, E. S.; Kadambala, R. S.; Zhang, C.; Brooks, J. S.; Wang, B.; Kramer, L. *Curr. Appl. Phys.* **2006**, *6*, 119.

(7) Wang, Z.; Liang, Z.; Wang, B.; Zhang, C.; Kramer, L. *Compos. Part A-Appl.* **2004**, *35*, 1225.

(8) Polyakov, B.; Daly, B.; Prikulis, J.; Lisauskas, V.; Vengalis, B.; Morris, M. A.; Holmes, J. D.; Erts, D. *Adv. Mater.* **2006**, *18*, 1812.

Chapter 7: Conclusions and Future Directions

7.1 YOUNG'S MODULUS AND MECHANICAL QUALITY FACTORS OF GERMANIUM NANOWIRE RESONATORS

7.1.1 Conclusions

Suspended clamped-free germanium (Ge) nanowire beams were fabricated on the edge of copper transmission electron microscopy (TEM) grids. Fabrication was performed using a nanomanipulation system inside of a dual beam scanning electron microscope / focused ion beam (SEM/FIB) system. The nanowires were drop casted from a toluene suspension onto lacey carbon TEM grids and allowed to air dry. Nanowires which fell partially over the copper TEM grid and partially over the lacey carbon were located using SEM mode. The nanomanipulation system was used to physically remove the lacey carbon from beneath the nanowires with an electrochemically-sharpened tungsten probe followed by "spot welding" the fixed end of the nanowire to the copper grid by electron beam-induced deposition of platinum. SEM and TEM were used to determine the length and diameter of the cantilever, respectively.

Two tungsten probes were used to excite the cantilevered Ge nanowire into vibration. The nanomanipulator was used to position one end of the nanowire on the copper TEM grid and the other within a micrometer of the nanowire tip. A sinusoidal voltage of 100 mV was applied to the two tungsten probes. The nanowire was monitored in SEM mode as the frequency was swept until the nanowire was observed to vibrate.

15-20 SEM images were taken over the range of vibration in order to fully capture the frequency-dependent amplitude of vibration.

The fundamental resonance frequency and mechanical quality factor were measured for Ge nanowire cantilevers with diameters varying from 50 to 140 nm. The Young's modulus was found to be independent of diameter and *Q* decreased with decreasing diameter. The nanowires of differing diameter studied exhibit no observable difference in crystal quality or surface chemistry. Thus, the mechanical properties related to the Ge-Ge bonding in the core of the wire, such as *E*, do not differ from that of the bulk material when the diameters are in this size range. The Ge nanowires studied clearly indicate that smaller diameter decreases *Q*, and that this is undoubtedly a fundamental trend of nanometer-scale resonators. The absolute value of *Q*, however, depends strongly on the surface chemistry and surface structure of the cantilever material and wide variations in *Q* have been observed, such as the recent ultrahigh *Q* values of 13,000 measured by Feng, et al.[1] for "pristine" 80 nm diameter Si nanowire cantilevers that are two orders of magnitude higher than the *Q* values of the Ge nanowires studied here. Clearly, the underlying surface chemistry and surface structure underlie how energy dissipates from oscillating nanoelectromechanical resonators and is currently a research topic that requires much greater study and understanding.

7.1.2 Future Directions

Although the Ge nanowires in this work didn't reveal any dependence of Young's modulus on the diameters of the nanowires, further research is needed to obtain measurements of nanowires below 50 nm. Ge nanowires below 10 nm are readily

produced by the synthesis method described in Chapter 2.[2,3] However, the currently described technique whereby lacey carbon is removed from beneath the nanowires was found to break smaller diameter nanowires. Future work should focus on developing new techniques for fabricating suspended beam resonators from the Ge nanowires with diameters below 10 nm.

Clamped-clamped beams with electronic transduction or resonant behavior can be explored in an effort to reduce the errors inherent to the post image processing used herein to determine the vibration amplitude. In Figure 7.1, an SEM of a prototype suspended clamped-clamped beam NEMS device is shown. The device was fabricated by an initial photolithography, deposition, and liftoff step to produce gold electrodes on a substrate. Ion beam etching was used to mill a trench between the large gold electrode pads using the ion beam mode in the dual beam SEM/FIB system. The nanowire was positioned over the trench using the nanomanipulator. Electrical connections were made using ion beam-induced deposition of platinum to produce low resistance contacts. A variety of methods are available to electronically transduce the motion of these types of structures including magnetomotive, capacitive, and piezoelectric detection.[4-6] This type of device would allow for experimental investigation of the effect of surface passivation on Q, the sensing capabilities of the devices exposed to various analytes, temperature dependence, and many others.

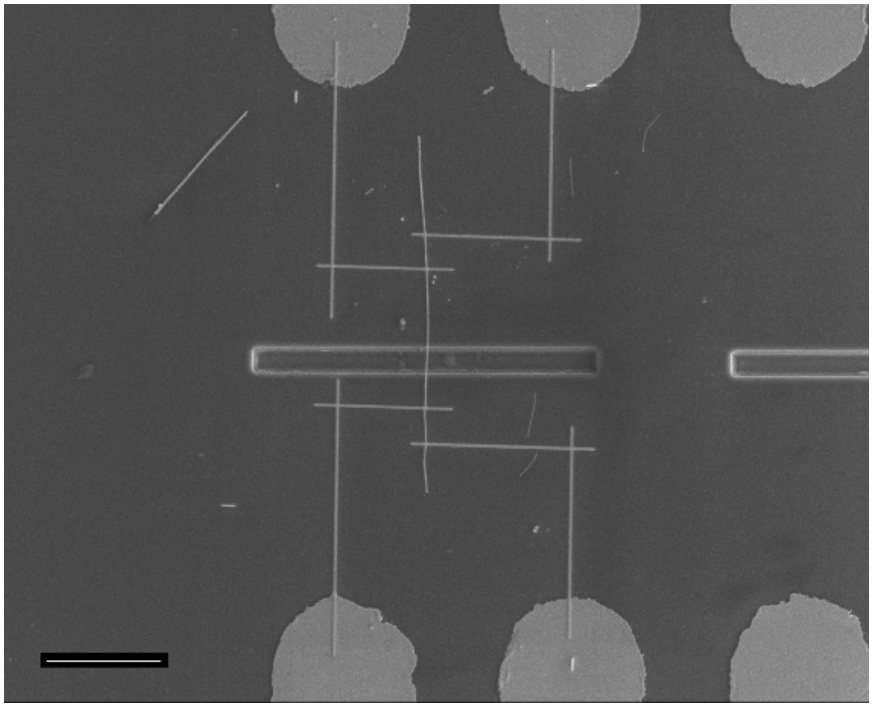

Figure 7.1 SEM image of Ge nanowire suspended over an ion beam etched trench on a silicon dioxide substrate. The Ge nanowire is connected to larger gold electrode pads by platinum lines written by ion beam-induced deposition inside of a dual beam SEM/FIB. (Scale bar is 5 μm)

7.2 GERMANIUM NANOWIRE STRENGTH AND FLEXIBILITY

7.2.1 Conclusions

The maximum radius of curvature and flexural strain of suspended Ge nanowires between 23 and 97 nm in diameter were measured by bending with tungsten probes to the point of fracture. The Ge nanowires are extremely flexible, allowing bending down to a 67 nm radius of curvature for the smallest diameter. Ge nanowires were found to tolerate exceptionally high strains up to 17 %, well in excess of the values of bulk Ge. The maximum radius of curvature and maximum strain increased with decreasing nanowire

diameter expected from a decrease in defects in the reduced volume of the material. The bending strengths of Ge nanowires were determined and found to equal the theoretical fracture strengths of a defect-free, perfect crystalline solid as their diameters were reduced. Room temperature plasticity was also observed at extremely high strains. Plastically deformed Ge nanowires exhibited amorphization at the point of maximum strain.

7.2.2 Future Directions

In order to further investigate the plastic behavior of Ge nanowires, experiments will need to be designed which controllably deform the nanowires while observing changes in the crystal structure. This has been accomplished in recent studies of silicon and silicon carbide nanowires by in situ TEM studies using polymer films which contract inside of the TEM.[7-9] Alternatives include the use of in situ TEM nanomanipulation experiments or the use of a MEMS test platform for nanowire loading inside of a TEM.

7.3 OPTICAL PROPERTIES OF GERMANIUM NANOWIRE COMPOSITES AND DISPERSIONS

7.3.1 Conclusions

Ge nanowire-polymer composites and well-dispersed PEGylated Ge nanowires in solution were used to measure the optical properties of the nanowires. The absorbance spectra of the nanowires were found to have markedly different behavior from their bulk counterpart. A coupled dipole method, the DDA, was used to explain the presence of peaks in the absorbance spectra and the difference in the material's dependence on

energy by using a simple model of an individual Ge nanowire. Simulations showed extinction spectra that depend significantly on the size of the nanowires and the incident electric field polarization. Modeling of an average size nanowire with an approximation to incident randomly polarized light impinging on randomly oriented nanowires displayed qualitative agreement with the experimental spectra. A major peak at 600 nm wavelengths can be attributed to a resonant optical mode in the individual nanowires leading to enhanced absorption by acting as a subwavelength optical trap. The simulation results demonstrate the potential to engineer the absorption and light trapping behavior of semiconductor nanowire devices and films by tuning their size-, shape-, and orientation-dependent optical interactions.

7.3.2 Future Directions

The fabrication of composites composed of nanowires in an elastomer opens up the possibility of testing the polarization-dependent absorbance of strained composites. Under strain, the nanowires experience mechanical forces which align the wires parallel to the applied force. Absorbance measurements with polarizations parallel and perpendicular to the applied force should reveal drastically different behavior.

In addition, the mechanical testing of the composites will reveal their potential as fiber reinforcements. Given the mechanical and optical properties reported here in, these measurements could further reveal their potential for the production of multifunctional composites. Initial investigations of the mechanical properties of Ge nanowire composites provided inconclusive data due to slippage of the material in the clamps of the apparatus (Figure 7.3).

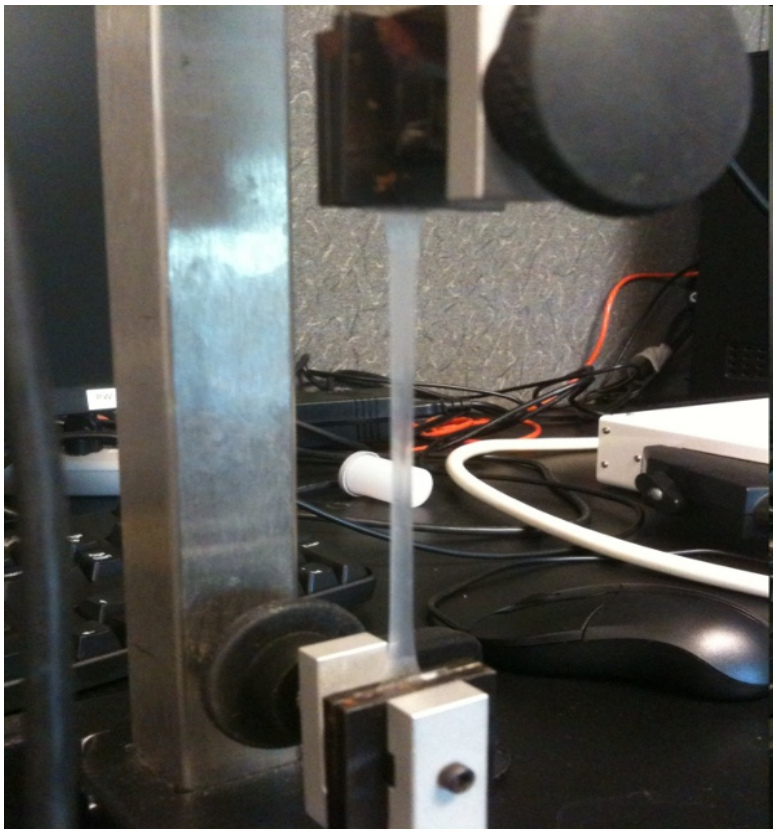

Figure 7.2 Photograph of Ge nanowire-polymer composite strained under a tensile load.

7.4 GERMANIUM NANOWIRE NONWOVEN FABRIC

7.4.1 Conclusions

A Ge nanowire nonwoven fabric of varying thickness was made by vacuum filtration of different volumes of nanowires dispersed in toluene. The solutions were filtered through porous alumina filters and subsequently dried under vacuum. The fabric formed is 1 % of the density of bulk Ge and contains 10 % wires and 90 % void space by volume. The fabric was mechanically stable, enabling handling and manipulation for

testing. Additionally, the fabric was found to be photoconductive with a 200 % increase in conductivity under 1 sun, AM 1.5 G light conditions.

7.4.2 Future Directions

In previous studies, the Ge nanowires produced by the SFLS method yielded nanowires which were intrinsically p-type without any intentional doping.[10] Infusion of n-type polymers or incorporation of multiple layers of nanowires with different dopings could lead to fabrics with photovoltaic, light-emitting, or other novel properties.

Moreover, techniques currently used for electric or magnetic field alignment in CNT fabrics and paper could be utilized to further tune nanowire orientation-tunable optical properties demonstrated through the simulations in Chapter 5.[11]

7.5 REFERENCES

(1) Feng, X. L.; Rongui, H.; Yang, P.; Roukes, M. L. *Nano Lett.* **2007**, *7*, 1953.

(2) Hanrath, T.; Korgel, B. A. *J. Am. Chem. Soc.* **2002**, *124*, 1424.

(3) Hanrath, T.; Korgel, B. A. *Adv. Mater.* **2003**, *15*, 437.

(4) Gaillard, J.; Skove, M.; Rao, A. M. *Appl. Phys. Lett.* **2005**, *86*, 233109.

(5) Ke, C.; Espinosa, H. D. In *Handbook of Theoretical and Computational Nanotechnology*; American Scientific Publishers: 2005.

(6) Sazonanova, V.; Yalsh, Y.; Ustunel, H.; Roundy, D.; Arias, T. A.; McEuen, P. L. *Nature* **2004**, *431*, 284.

(7) Han, X.; Zheng, K.; Zhang, Y. F.; Zhang, X.; Zhang, Z.; Wang, Z. L. *Adv. Mater.* **2007**, *19*, 2112.

(8) Han, X. D.; Zhang, Y. F.; Zheng, K.; Zhang, X. N.; Zhang, Z.; Hao, Y. J.; Guo, X. Y.; Yuan, J.; Wang, Z. L. *Nano Lett.* **2007**, *7*, 452.

(9) Zheng, K.; Han, X.; Wang, L.; Zhang, Y.; Yue, Y.; Qin, Y.; Zhang, X.; Zhang, Z. *Nano Lett.* **2009**, *9*, 2471.

(10) Hanrath, T.; Korgel, B. A. *J. Phys. Chem. B* **2005**, *109*, 5518.

(11) Gonnet, P.; Liang, Z.; Choi, E. S.; Kadambala, R. S.; Zhang, C.; Brooks, J. S.; Wang, B.; Kramer, L. *Curr. Appl. Phys.* **2006**, *6*, 119.

BIBLIOGRAPHY

Agarwal, R.; Lieber, C. M. Appl. Phys. A-Mater. 2006, 85, 209-215.

Bahr, J. L.; Yang, J.; Kosynkin, D. V.; Bronikowski, M. J.; Smalley, R. E.; Tour, J. M. J. Am. Chem. Soc. 2001, 123, 6536.

Barrett, C. R.; Nix, W. D.; Tetelman, A. S. The Principles of Engineering Materials; Prentice-Hall, Inc.: Englewood Cliffs, NJ, 1973.

Bashouti, M.; Salalha, W.; Brumer, M.; Zussman, E.; Lifshitz, E. ChemPhysChem 2006, 7, 102.

Borchi, E.; Gennaro, S. D.; Macii, R.; Zoli, M. J. Phys. D: Appl. Phys. 1988, 21, 1304.

Broughton, J. Q.; Meli, C. A. Phys. Rev. B 1997, 56, 611.

Brust, M.; Walker, M.; Bethell, D.; Schiffrin, D. J.; Whyman, R. J. J. Chem. Soc., Chem. Commun. 1994, 801, 1994.

Cammarata, R. C. Progr. Surf. Sci. 1994, 46, 1.

Cao, L.; White, J. S.; Park, J. S.; Schuller, J. A.; Clemens, B. M.; Brongersma, M. L. Nat. Mater. 2009, 8, 643.

Carr, D. W.; Evoy, S.; Sekaric, L.; Craighead, H. G.; Parpia, J. M. Appl. Phys. Lett. 1999, 75, 920.

Chen, C. Q.; Shi, Y.; Zhang, Y. S.; Zhu, J.; Yan, Y. J. Phys. Rev. Lett. 2006, 96, 075505.

Chen, G.; Wu, J.; Lu, Q.; Gutierrez, H. R.; Xiong, Q.; Pellen, M. E.; Petko, J. S.; Werner, D. H.; Eklund, P. C. Nano Lett. 2008, 8, 1341.

Chen, X.; Zhang, S.; Wagner, G. J.; Ding, W.; Ruoff, R. S. J. Appl. Phys. 2004, 95, 4823.

Chokski, A. H.; Rosen, A.; Karch, J.; Gleiter, H. Scr. Metall. 1989, 23, 1679.

Cimalla, V.; Niebelschutz, F.; Tonisch, K.; Foerster, C.; Brueckner, K.; Cimalla, I.; Friedrich, T.; Pezoldt, J.; Stephan, R.; Hein, M.; Ambacher, O. Sens. Actuators, B 2007, 126, 24.

Claeys, C. Germanium-Based Technologies: From Materials to Devices; Elsevier Science: Oxford, 2007.

Clarke, D. R. In The Mechanical Properties of Semiconductors; Faber, K. T., Malloy, K. J., Eds.; Academic Press, Inc.: San Diego, CA, 1992; Vol. 37.

Cuenot, S.; Fretigny, C.; Demoustier-Champagne, S.; Nysten, B. Phys. Rev. B 2004, 69, 165410.

Cui, Y.; Lauhun, L. J.; Gudiksen, M. S.; Wang, J.; Lieber, C. M. Appl. Phys. Lett. 2001, 78, 2214.

Davidson III, F. M.; Lee, D. C.; Fanfair, D. D.; Korgel, B. A. J. Phys. Chem. C 2007, 111, 2929.

Dikin, D. A.; Chen, X.; Ding, W.; Wagner, G.; Ruoff, R. S. J. Appl. Phys. 2003, 93, 226.

Dowling, N. E. Mechanical Behaviour of Materials; Prentice Hall: Englewood Cliffs, NJ, 1999.

Draine, B. T. Astrophysical J. 1988, 333, 848.

Draine, B. T.; Flatau, P. J. J. Opt. Soc. Am. A 1994, 11, 1491.

Ekinci, K. L.; Roukes, M. L. Rev. Sci. Instrum. 2005, 76, 061101.

Endo, M.; Muramatsu, H.; Hayashi, T.; Kim, Y. A.; Terrones, M.; Dresselhaus, M. S. Nature 2005, 433, 476.

Evans, C. C. Whiskers; Mills and Boon: London, 1972.

Fanfair, D. D.; Korgel, B. A. Cryst. Growth Des. 2005, 5, 1971.

Fanfair, D. D.; Korgel, B. A. Cryst. Growth Des. 2008, 8, 3246.

Feng, X. L.; Rongui, H.; Yang, P.; Roukes, M. L. Nano Lett. 2007, 7, 1953.

Fowles, G. R.; Cassiday, G. R. Analytical Mechanics. Hartcourt, Inc.: Florida, 1999.

Gaillard, J.; Skove, M.; Rao, A. M. Appl. Phys. Lett. 2005, 86, 233109.

Gaspar, J.; Chu, V.; Conde, J. P. Appl. Phys. Lett. 2004, 84, 622.

Gonnet, P.; Liang, Z.; Choi, E. S.; Kadambala, R. S.; Zhang, C.; Brooks, J. S.; Wang, B.; Kramer, L. Curr. Appl. Phys. 2006, 6, 119.

Gordon, M. J.; Baron, T.; Dhalluin, F.; Gentile, P.; Ferret, P. Nano Lett. 2009, 9, 525.

Greytak, A. B.; Barrelet, C. J.; Li, Y.; Lieber, C. M. Appl. Phys. Lett. 2005, 87, 151103.

Gurtin, M. E.; Murdoch, A. Arch. Ration. Mech. Anal. 1975, 57, 291.

Hall, E. O. Proc. Phys. Soc. B 1951, 64, 747.

Han, X. D.; Zhang, Y. F.; Zheng, K.; Zhang, X. N.; Zhang, Z.; Hao, Y. J.; Guo, X. Y.; Yuan, J.; Wang, Z. L. Nano Lett. 2007, 7, 452.

Han, X.; Zheng, K.; Zhang, Y. F.; Zhang, X.; Zhang, Z.; Wang, Z. L. Adv. Mater. 2007, 19, 2112.

Hanrath, T.; Korgel, B. A. Adv. Mater. 2003, 15, 437.

Hanrath, T.; Korgel, B. A. J. Am. Chem. Soc. 2002, 124, 1424.

Hanrath, T.; Korgel, B. A. J. Am. Chem. Soc. 2004, 126, 15466.

Hanrath, T.; Korgel, B. A. J. Phys. Chem. B 2005, 109, 5518.

Hanrath, T.; Korgel, B. A. Small 2005, 1, 717-721.

He, R.; Yang, P. Nature 2006, 1, 42.

Heidelberg, A.; Ngo, L. T.; Wu, B.; Phillips, M. A.; Sharma, S.; Kamins, T. I.; Sader, J. E.; Boland, J. J. Nano Lett. 2006, 6, 1101.

Herring, C. The Physics of Powder Metallurgy. McGraw-Hill Book Company, Inc.: New York, 1951.

Herring, C.; Galt, J. K. Phys. Rev. 1952, 85, 1060-1061.

Hoffmann, S.; Utke, I.; Moser, B.; Michler, J.; Christiansen, S. H.; Schmidt, V.; Senz, S.; Werner, P.; Gosele, U.; Gallif, C. Nano Lett. 2006, 6, 622.

Holmes, J. D.; Johnston, K. P.; Doty, R. C.; Korgel, B. A. Science 2000, 287, 1471.

Hsin, C. L.; Mai, W.; Gu, Y.; Gao, Y.; Huang, C. T.; Liu, Y.; Chen, L. J.; Wang, Z. L. Adv. Mater. 2008, 20, 1.

Hu, L.; Chen, C. Q. Nano Lett. 2007, 7, 3249.

Ibach, H. J. Vac. Sci. Technol. A 1994, 12, 2240.

Johnson, J. C.; Choi, H. J.; Knutsen, K. P.; Schaller, R. D.; Yang, P.; Saykally, R. J. Nat. Mater. 2002, 1, 106.

Ke, C.; Espinosa, H. D. In Handbook of Theoretical and Computational Nanotechnology; American Scientific Publishers: 2005.

Korgel, B. A. Nature Mater. 2006, 5, 521.

Kumar, S.; Wang, Y. In Composites Engineering Handbook; Mallick, P. K., Ed.; Marcel Dekker, Inc.: New York, 1997.

Law, M.; Goldberger, J.; Yang, P. Annu. Rev. Mater. Res. 2004, 34, 83.

Law, M.; Joshua, G.; Yang, P. Annu. Rev. Mater. Res. 2004, 34, 83-122.

Law, M.; Sirbuly, D. J.; Johnson, J. C.; Goldberger, J.; Saykally, R. J.; Yang, P. Science 2004, 305, 1269.

Lee, B.; Rudd, R. E. Phys. Rev. B 2007, 75, 041305.

Lee, K.; Lukic, B.; Magrez, A.; Seo, J. W.; Briggs, G. A. D.; Kulik, A. J.; Forro, L. Nano Lett. 2007, 7, 1598.

Li, X.; Ono, T.; Wang, Y.; Esashi, M. Appl. Phys. Lett. 2003, 83, 3081.

Liu, K. H.; Wang, W. L.; Xu, Z.; Liao, L.; Bai, X. D.; Wang, E. G. Appl. Phys. Lett. 2006, 89, 221908.

Lukic, B.; Seo, J. W.; Bacsa, R. R.; Delpeux, S.; Beguin, F.; Bister, G.; Fonseca, A.; Nagy, J. B.; Kis, A.; Jeney, S.; Kulik, A. J.; Forro, L. Nano Lett. 2005, 5, 2075.

Macmillan, N. H. J. Mater. Sci. 1972, 7, 239.

Maeda, Y.; Tsukamoto, N.; Yazawa, Y.; Kanemitsu, Y.; Masumoto, Y. Appl. Phys. Lett. 1991, 59, 3168.

McSkimin, H. J. J. Appl. Phys. 1953, 24, 988.

Meirovitch, L. Analytical Methods in Vibrations. The Macmillan Company: New York, 1967.

Menon, M.; Srivastava, D.; Ponomareva, I.; Chernozatonski, L. A. Phys. Rev. B 2004, 70, 125313.

Miller, R. E.; Shenoy, V. B. Nanotech. 2000, 11, 139-147.

Muskens, O. L.; Diedenhofen, S. L.; Kaas, B. C.; Algra, R. E.; Bakkers, E. P. A. M.; Rivas, J. G.; Lagendijk, A. Nano Lett. 2009, 9, 930.

Muskens, O. L.; Diedenhofen, S. L.; Weert, M. H. M.; Borgstrom, M. T.; Bakkers, E. P. A. M.; Rivas, J. G. Adv. Funct. Mater. 2008, 18, 1039.

Muskens, O. L.; Rivas, J. G.; Algra, R. E.; Bakkers, E. P. A. M.; Lagendijk, A. Nano Lett. 2008, 8, 2638.

Nam, C. Y.; Jaroenapibal, P.; Tham, D.; Luzzi, D. E.; Evoy, S.; Fischer, J. E. Nano Lett. 2006, 6, 153.

Namazu, T.; Isono, Y.; Tanaka, T. J. Microelectromech. S. 2000, 9, 450.

Ngo, L. T.; Almecija, D.; Sader, J. E.; Daly, B.; Petkov, N.; Holmes, J. D.; Erts, D.; Boland, J. J. Nano Lett. 2006, 6, 2964.

Nieman, G. W.; Weertman, J. R.; Siegel, R. W. Scr. Metall. 1989, 23, 2013.

Nilsson, S. G.; Borrise, X.; Montelius, L. Appl. Phys. Lett. 2004, 85, 3555.

Oliver, D. J.; Bradby, J. E.; Williams, J. S. J. Appl. Phys. 2007, 101, 043524.

Park, H. S.; Cai, C.; Espinosa, H. D.; Huang, H. MRS Bull. 2009, 34, 178.

Pauzauskie, P. J.; Yang, P. Mater. Today 2006, 9, 36-45.

Pearson, G. L.; Read, W. T.; Feldmann, W. L. Acta. Metall. 1957, 5, 181.

Petch, N. J. J. Iron Steel Inst. 1953, 174, 25.

Petrovic, J. J.; Hoover, R. C. J. Mater. Sci. 1987, 22, 517.

Petrovic, J. J.; Milewski, J. V.; Rohr, D. L.; Gac, F. D. J. Mater. Sci. 1985, 20, 1167.

Podolskiy, V. A. J. Nonlinear Opt. Phys. 2002, 11, 65.

Polyakov, B.; Daly, B.; Prikulis, J.; Lisauskas, V.; Vengalis, B.; Morris, M. A.; Holmes, J. D.; Erts, D. Adv. Mater. 2006, 18, 1812.

Poncharal, P.; Wang, Z. L.; Ugarte, D.; deHeer, W. A. Science 1999, 283, 1513.

Qian, D.; Wagner, G. J.; Liu, W. K.; Yu, M. F.; Ruoff, R. S. Appl. Mech. Rev. 2002, 55, 495.

Roesler, J.; Harders, H.; Baeker, M. Mechanical Behaviour of Engineering Materials; Springer: New York, 2007.

Ruoff, R. S.; Lorents, D. C. Carbon 1995, 33, 925.

Ruoff, R. S.; Qian, D.; Liu, W. K. C. R. Physique 2003, 4, 993.

Salvetat, J. P.; Andrew, G.; Briggs, D.; Bonard, J. M.; Bacsa, R. R.; Kulik, A. J.; Stockli, T.; Burnham, N. A.; Forro, L. Phys. Rev. Lett. 1999, 82, 944.

Sazonanova, V.; Yalsh, Y.; Ustunel, H.; Roundy, D.; Arias, T. A.; McEuen, P. L. Nature 2004, 431, 284.

Shah, P. S.; Hanrath, T.; Johnston, K. P.; Korgel, B. A. J. Phys. Chem. B 2004, 108, 9574-9587.

Sharma, P.; Ganti, S.; Bhate, N. Appl. Phys. Lett. 2003, 82, 535-537.

Smith, D. A.; Holmberg, V. C.; Lee, D. C.; Korgel, B. A. J. Phys. Chem. C 2008, 112, 10725.

Smith, P. A.; Nordquist, C. D.; Jackson, T. N.; Mayer, T. S.; Marin, B. R. Appl. Phys. Lett. 2000, 77, 1399.

Sze, S. M. Physics of Semicoductor Devices; John Wiley: New York, 1981.

Tabib-Azar, M.; Nassirou, M.; Wang, R. Appl. Phys. Lett. 2005, 87, 113102.

Tan, E. P. S.; Lim, C. T. Compos. Sci. Technol. 2005, 66, 1102.

Tsakalakos, L.; Balch, J.; Fronheiser, J.; Shih, M. Y.; LeBoeuf, S. F.; Pietrzykowski, M.; Codella, P. J.; Korevaar, B. A.; Sulima, O.; Rand, J.; Davuluru, A.; Rapol, U. J. Nanophotonics 2007, 1, 013552.

Wang, J.; Gudiksen, M. S.; Duan, X.; Cui, Y.; Lieber, C. M. Science 2001, 293, 1455.

Wang, Y.; Henry, J. A.; Debodhonyaa, S.; Hines, M. A. Appl. Phys. Lett. 2004, 85, 5736.

Wang, Z.; Liang, Z.; Wang, B.; Zhang, C.; Kramer, L. Compos. Part A-Appl. 2004, 35, 1225.

Whang, D.; Jin, S.; Wu, Y.; Lieber, C. M. Nano Lett. 2003, 3, 1255.

Wong, E. W.; Sheehan, P. E.; Lieber, C. M. Science 1997, 277, 1971.

Wortman, J. J.; Evans, R. A. J. Appl. Phys. 1965, 36, 153.

Wu, B.; Heidelberg, A.; Boland, J. J. Nature 2005, 4, 525.

Wu, Y.; Yang, P. J. Am. Chem. Soc. 2001, 123, 3165.

Xu, G. In Dislocations in Solids; Nabarro, F. R. N., Hirth, J. P., Eds.; North Holland, 2004; Vol. 12, p 83.

Yang, J.; Ono, T.; Esashi, M. Appl. Phys. Lett. 2000, 77, 3860.

Yang, J.; Ono, T.; Esashi, M. J. Microelectromech. S. 2002, 11, 775.

Yang, P. Nature 2003, 425, 243.

Yasumura, K. Y.; Stowe, T. D.; Chow, E. M.; Pfafman, T.; Kenny, T. W.; Stipe, B. C.; Rugar, D. J. Microelectromech. S. 2000, 9, 117.

Yurkin, M. A.; Hoekstra, A. G. J. Quant. Spectrosc. Ra. 2007, 106, 558.

Zener, C. Phys. Rev 1938, 53, 90-99.

Zheng, K.; Han, X.; Wang, L.; Zhang, Y.; Yue, Y.; Qin, Y.; Zhang, X.; Zhang, Z. Nano Lett. 2009, 9, 2471.

VITA

Damon Smith was born in Leesville, LA on October 31, 1973. After graduating from Northshore High School in Slidell, LA in 1991, Damon moved to New Orleans to pursue artistic and musical interests. In 1998, he entered the University of New Orleans as an undergraduate and received a B.S. in Physics in 2003. After undergraduate studies, Damon stayed at UNO and received his M.S. in Applied Physics in 2005. He entered graduate school at the University of Texas at Austin in 2005 to pursue a PhD degree in Materials Science and Engineering while studying the properties of semiconductor nanowires in Dr. Brian Korgel's research group in the Chemical Engineering department.

Permanent Address: 5706 Duval St. Austin, TX 78752

This dissertation was typed by the author.